Climate and the Evolution of the Ocean: The Paleoceanographic Data

Thibaut Caley, Natalia Vázquez Riveiros, Laurent Labeyrie, Elsa Cortijo, Jean-Claude Duplessy

Chapter 21

Climate and the evolution of the ocean: the paleoceanographic data

Thibaut Caley[1*], Natalia Vázquez Riveiros[2,3*], Laurent Labeyrie[2,4*], Elsa Cortijo[2] and Jean-Claude Duplessy[2]

***These authors have contributed equally to this chapter.**

[1] *EPOC, UMR 5805, CNRS, University of Bordeaux, Pessac, France.*

[2]*Laboratoire des Sciences du Climat et de l'Environnement, LSCE/IPSL, CEA-CNRS-UVSQ, Université Paris-Saclay, 91190 Gif-sur-Yvette, France.*

[3]*Institut Français de Recherche pour l'Exploitation de la Mer (Ifremer), Unité de Geosciences Marines, Pointe du Diable, 29280, Plouzané, France*

[4]*now at LGO Université Bretagne Sud-56000 Vannes*

21.1 Introduction: the development of tools and concepts

The idea of reconstructing the history of oceans and climates in the past using marine sediment cores arrived quite late after the beginnings of oceanography. It was initiated in the twentieth century, well after the first attempts to measure variations in seawater temperature down the water column, which date back to the eighteenth century with the great circumnavigation expeditions. Land geologists were the first to propose paleoceanographic reconstructions from exposed marine series, limiting the collected information to former coastal waters. The first reconstructions of past seawater temperatures were made possible by the piston corer developed by the Swedish oceanographer Kullenberg, capable of collecting continuous sedimentary deposits without layer disruption. Geologists were therefore able to collect uninterrupted sedimentary series, sometimes over 20 m in length, for laboratory analysis, and thus study long records of the environmental conditions from the time the sediments were deposited. With this type of corer, the Swedish expedition of 1947-1948 collected over 300 different cores from various deep ocean basins that became the basis of the first studies on the geological history of the oceans. In parallel, during the 1950s, Maurice Ewing, the founder of the Lamont-Doherty Geological Observatory (USA), and one of the developers of seismic sediment mapping of the ocean floor, initiated the first systematic

collection of marine sediment cores. The first descriptions of the main sedimentary systems, changes in fossil faunas and the timeframe for the first biostratigraphic age scales were proposed based on these cores. One of the main results of these studies was the continuous reconstruction of the alternating warm and cold phases that took place during the Pleistocene.

Unquestionably, the honor for the initiation of quantitative paleoceanography belongs to Cesare Emiliani. After the discovery of isotopic fractionation and the development of an accurate method to measure isotopic ratios, Harold Urey and his group in Chicago refined the use of the isotopic ratio $^{18}O/^{16}O$ in fossil carbonates as a paleothermometer. They realized that the $^{18}O/^{16}O$ ratio of foraminiferal shells and other carbonates depended on two variables: the temperature and the $^{18}O/^{16}O$ ratio of the water where the carbonate was formed. Changes in water temperature are reflected in variations in the isotopic fractionation between the carbonate and the water during the formation of the shell: for water with a given isotopic composition, the higher the temperature, the lower the $^{18}O/^{16}O$ ratio (Epstein *et al.*, 1951; 1953). Emiliani (1955) applied this tool to foraminifera shells sampled along a sediment core from the Caribbean Sea to propose the first reconstruction of the variations in sea surface temperature (SST) over the past 400 ka (Fig. 21.1). He also established the major methodological guidelines for this type of study: use of continuous records, precise dating, and interpretation of parameters quantitatively linked to key variables of the climate system.

To extract a temperature signal from the $^{18}O/^{16}O$ ratio of planktonic foraminifera, Emiliani had to constrain the changes in the isotopic composition of the ocean water in which the foraminifera developed. The $^{18}O/^{16}O$ ratio of seawater is affected by evaporation and precipitation: the vapor phase is depleted in the heavy ^{18}O isotopes relative to the liquid phase. Conversely, when the water vapor in clouds condenses, the precipitation is richer in ^{18}O than the vapor. Thus, the transport of air masses from low to high latitudes is accompanied by a large-scale isotopic distillation process in the water vapor that results in the gradual decline of the $^{18}O/^{16}O$ ratio in precipitation. For this reason, the $^{18}O/^{16}O$ ratio of snowfall feeding the high-latitude ice caps is depleted by more than 30‰ compared to that of the tropical ocean.

A

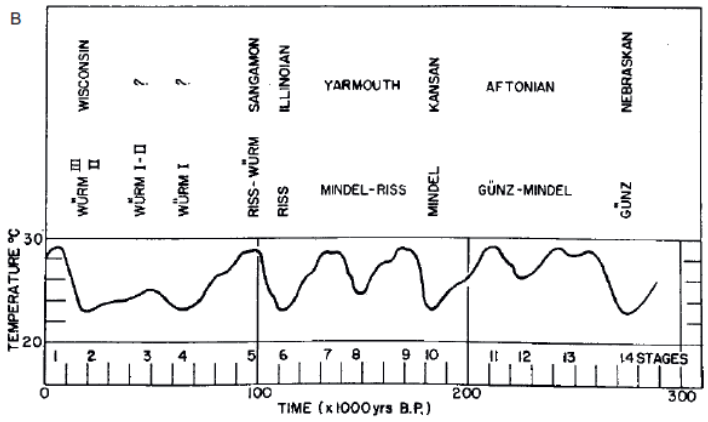

Fig. 21.1 – A. Cesare Emiliani, founder of isotopic marine paleoclimatology, in the early 1950s at the University of Chicago. (Photo from the archives of the Rosenstiel School of Marine and Atmospheric Science, University of Miami). B. First attempt to evaluate surface water temperature changes in the Caribbean Sea, Emiliani (1955). Subsequent studies have shown that the timescale was underestimated by about 25% (the last interglacial, called Sangamon in American literature, is dated at about 125 000 years and not 100 000 years), and that the amplitude of temperature variations, calculated from a simple model (see below), was overestimated.

The growth and melting of ice caps, which involves considerable volumes of water (several million cubic kilometers), directly affect the salinity and the average $^{18}O/^{16}O$ ratio of the ocean, and therefore that of the foraminifera that develop there. Regional climate changes are also accompanied by local variations in evaporation and precipitation, which induce further regional variations in the salinity of surface seawater and its $^{18}O/^{16}O$ ratio.

From the data available at the time, Emiliani (1955) estimated that the development of large ice sheets covering Canada (the Laurentide ice sheet) and northern Europe (the Fennoscandian ice sheet) at the maximum of the glaciation caused an enrichment in ^{18}O of the global ocean of + 0.4‰. We now know that the enrichment in ^{18}O in the glacial ocean was in fact close to + 1.0‰ (Schrag *et al.*, 2002). Despite these inaccuracies, the work of Emiliani was the first to demonstrate from paleoclimate observations that glacial – interglacial periods indeed oscillated with cyclicities predicted by the Milankovitch theory several decades earlier (see Chapter 7, Volume 2). Emiliani also proposed the 'Marine Isotopic Stage' (MIS) nomenclature, now universally adopted, to characterize the alternation of warm and cold Pleistocene phases, with odd numbers for interglacial periods and even numbers for glacial ones (1 for the Holocene, 2 for the last glacial period, and so on). He also discovered that the last interglacial, or MIS 5 (Fig. 21.1), was interrupted by two colder periods, which led him to divide it into three warm subperiods (designated 5a, 5c and 5e from the most recent to the oldest) and two cold ones (5b and 5d). The term '5e' is still frequently used, as it has been incorporated into the European continental reconstructions as the equivalent to the Eemian warm period. The isotopic stratigraphy formalism has since been generalized, with subdivisions either numbered as decimals between alternating warmer (*e.g.*, 5.1 for 5a, 5.3 for 5c and 5.5 for 5e) and colder (5.2 and 5.4) periods (Pisias *et al.*, 1984) or as letters (Railsback *et al.*, 2015).

With the assumption that past variations in foraminiferal $^{18}O/^{16}O$ ratios in cores from different ocean basins had to be approximately synchronous across global climate changes, Emiliani paved the way for a global marine isotopic stratigraphy. The demonstration that the volume of ice caps was indeed the dominant component of the isotopic signal recorded in marine cores reinforced the stratigraphic value of the marine isotopic stage age scale, which became a major reference tool for past climate change studies. The routine use of drilling ships as part of the International Ocean Drilling Program has allowed the recovery of sediment cores that cover the last tens of millions of years, extending the isotopic sequences not only to the Quaternary (Fig. 21.2), but as far back as the Paleocene, 60 Ma ago.

By 1970-1980, the paleoclimate community had arrived at the conclusion that variations in the oxygen isotopic composition provided a remarkable stratigraphic tool to establish long-term correlations. However, new tools still needed to be developed to precisely reconstruct past SST, as well as variations in other oceanic features such as salinity, or the direction and intensity of deep-water currents.

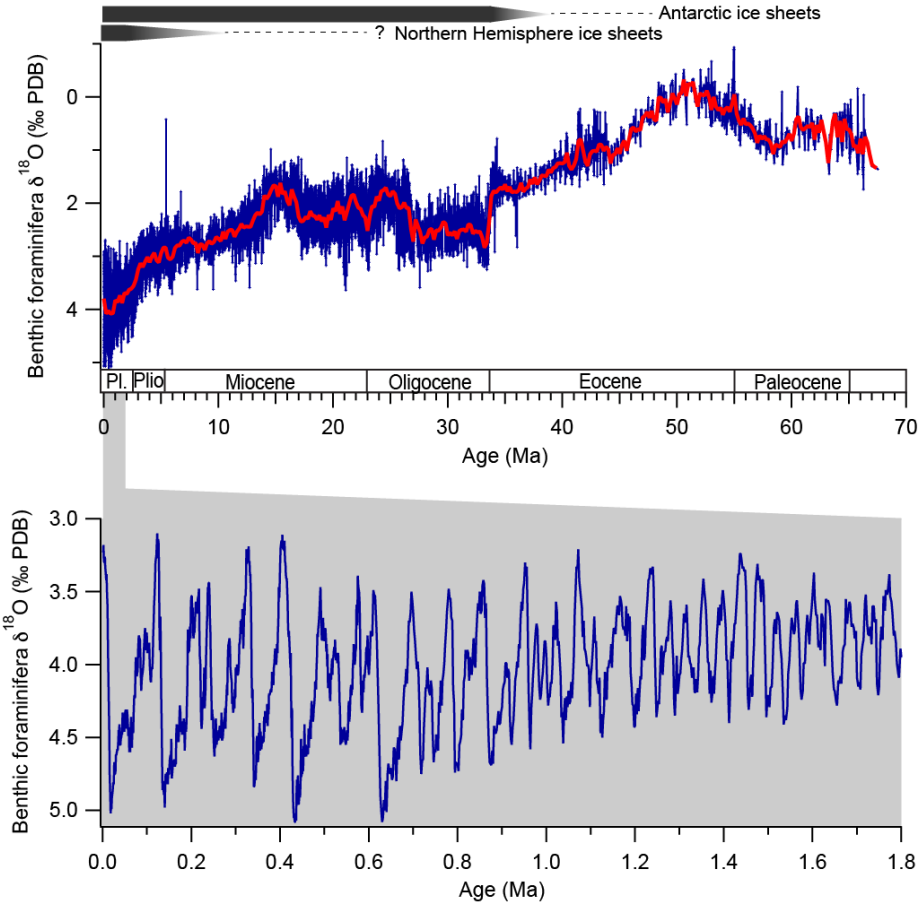

Fig. 21.2 - Variations in the isotopic composition of the oxygen in benthic foraminifera from 70 million years ago (Zachos *et al.*, 2008) with a detail of the last 1.8 Ma showing periodicities predicted by the astronomical theory of paleoclimate (Lisiecki and Raymo, 2005). Presence of Northern Hemisphere and Antarctic ice sheets are from Zachos *et al.*, (2008). Geological epochs (Pl. = Pleistocene, Plio = Pliocene) are indicated at the bottom of the top panel.

This chapter will focus on the development of classic and new paleoceanographic tracers

over the last decades. We will mainly, but not exclusively, focus on tracers that are based on foraminifera, since these abundant microfossils have been extensively used because of their ubiquity in the oceans and their great preservation potential. Their faunal associations and isotopic composition have been widely used as paleoclimate indicators for decades, and the advent of relatively new indicators implies an undiminished interest. Other indicators such as corals will be briefly discussed in association with some of the tracers.

21.2 Sea surface temperature

The surface temperature of the ocean is an essential climate parameter that governs heat exchange with the atmosphere. SST also modulates the solubility of gases, oxygen and CO_2 in particular, and their exchange rates with the atmosphere. The amplitude of the spatial variability of SST is well known: it ranges between -1.96 °C, freezing point for seawater at 35 psu, and 30°C to 35 °C, maximum temperature recorded for the open ocean. However, its temporal variability is more difficult to constrain because it not only varies on a daily basis, but also seasonally and annually. *In situ* measurement sensors are precise to ± 0.001 °C at a given location, water depth and time. Satellite data provide global coverage and allow long-term monitoring of the evolution of SST, but their accuracy is, at best, close to 0.1 °C, and surface values are averaged over tens or hundreds of square kilometers. Paleoceanographers cannot aim to reconstruct SST variations with this level of precision. Nonetheless, given the magnitude of changes in the past, relevant information may be acquired when SST changes are estimated to the nearest degree. Paleoceanographers also aim to estimate, whenever possible, the amplitude of the seasonal cycle, and the temperature distribution of the upper water column.

For these studies, two major types of paleotemperature indicators are used: (i) changes in the distribution of fossil planktonic flora or fauna (foraminifera, diatoms, dinoflagellates, radiolarians), and (ii) geochemical tracers produced by these organisms or recorded in their fossil skeletons.

21.2.1 The distribution of marine fauna and flora

The distribution of the various groups that make up the marine planktonic ecosystem was extensively studied during the major exploration campaigns that marked the nineteenth and early twentieth centuries. Foraminifera, single-celled protozoans that secrete a calcareous shell, were the most generally recorded group. They are very diverse and inhabit all the oceans, from the coldest to the warmest. However, each individual species has a limited tolerance to environmental changes, particularly temperature, which allowed biologists at the end of the nineteenth century to highlight the zonal distribution of many species. They also established existing relationships between climate and the abundance of certain species. These observations, along with the statistical method of ‘transfer functions’ developed by Imbrie and Kipp (see Chapter 10), served as a basis for the quantitative reconstruction of surface temperatures from fossil fauna found in marine sediments. Transfer functions allow the estimation of seawater temperature during both the cold and warm seasons, when adequate data is available. The basic principle for the reconstruction of SST changes in the past is to

assume that the ecological requirements of the species present nowadays have not changed since the past period under consideration. The specific abundance of planktonic foraminifera samples from recent core tops may be expressed as a matrix (*x* species relative distributions within each of *n* sampling stations) from which the vectors corresponding to the main factors that describe the specific faunal (or floral) variance can be extracted. The method proposed by Imbrie and Kipp (1971) provides the best correlation between changes in these factors and the associated changes within the modern environmental parameters, systematically selected for the *n* stations (such as summer and winter temperatures, or other parameters, provided they are statistically independent). A similar factor analysis, when applied to fossil assemblages down sediment cores, allows the paleotemperature to be estimated using the ecological equations calculated from the modern core tops. This work led to the great success of the CLIMAP group (Climate Long-range Investigation, Mapping And Prediction), which reconstructed the first global map of summer and winter SST distribution during the Last Glacial Maximum (LGM) period, about 21 ka ago (Fig. 21.3).

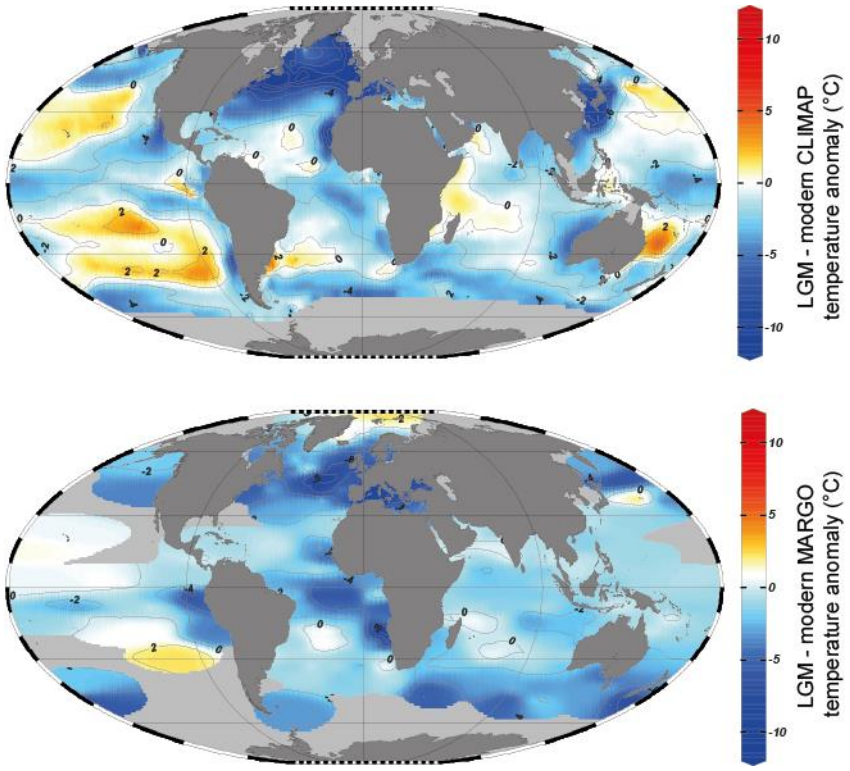

Fig. 21.3 – Reconstructions of temperature anomalies (°C) between the Last Glacial Maximum (LGM) and modern surface waters as obtained by the CLIMAP (1981) (August temperatures, top figure) and MARGO (2009) programs (July-August-September temperatures, bottom figure). While the two reconstructions have many features in common, the cores studied under the MARGO program revealed the presence of larger longitudinal gradients in SST in all ocean basins than the estimates of CLIMAP (1981).

One of the main problems with this paleo-reconstruction method is that it is based on the *a priori* stable statistical correlation between changes in the specific factors defined by the species distributions and the arbitrarily chosen environmental parameter, temperature, in this case. However, other environmental factors, such as the availability of food supply, may also

be involved and change the sensitivity of foraminifera to temperature from one region to another.

There is also another potential problem with the transfer function approach: it will provide accurate estimates only if modern conditions are good analogs of the past hydrological conditions. This is not always necessarily the case. For example, the fossil fauna of the eastern Mediterranean Sea during the LGM period has no modern analogs. Indeed, this basin experienced hydrological and climate conditions very different from the modern ones, due to the development of large ice sheets over Northern Europe and to a very different hydrological cycle. In fact, the absence of direct analogs becomes the rule rather than the exception for the distant past: most fossil species from periods earlier than the Quaternary are not found in recently deposited sediments.

This is why the method used by Imbrie and Kipp (1971) was gradually replaced by the *best analogs* method (see Chapter 10). Its principle is simple: to compare the changes in fossil assemblages to modern references, without a preconceived idea of the origin of the observed changes. The closest analogs are defined using a mathematical distance calculation. The method is based on the assumption that the closer a fossil assemblage is to one or more modern references, the more similar their optimal growth conditions are (temperature and nutrient supply, in particular). The distance to the best analogs and the dispersion of associated environmental conditions provide an estimate of the reconstruction uncertainties (Waelbroeck *et al.,* 1998).

In parallel with these statistical developments, recent advances in the field of artificial intelligence and neural networks have helped to improve paleoceanographic reconstructions without fundamentally changing the principle. Still based on the comparison between fossil fauna and modern reference fauna, they do not require the establishment of specific mathematical relationships, but establish their own learning from available databases through minimization of the uncertainties (Malmgren *et al.*, 2001).

These various methods, applied here to foraminifera, have also been used for diatom flora, coccoliths, dinoflagellate cysts and radiolarians. Diatoms, dominant in cold waters rich in silica, have been used in particular to reconstruct variations in sea ice cover in polar regions. The latest LGM SST global distribution, as reconstructed within the MARGO program, used several types of indicators and is presented in Fig. 21.3.

Statistical methods have many limitations: i) they can only be used if the faunal assemblages are close to modern assemblages; ii) the genetic diversity of species among different ocean regions may induce variations in their faunal responses to temperature and the corresponding statistical links; iii) temperature reconstructions based on variations in the abundance of fossil fauna or flora assume that other factors, such as productivity for example, have no significant influence on the relative abundances of the different species; iv) due to the activity of burrowing animals (bioturbation), marine sediments are usually mixed over several centimeters, so that the same stratigraphic level of a sediment core represents a mix of fauna that lived in different centuries (or even several thousand years apart if the sedimentation rate is low); v) transfer function calibration is based on the assumption that sediment core top

assemblages reflect modern hydrological conditions. This latest assumption ignores in particular ocean and climate changes which occurred over the last millennia, and that could have been significant enough to bias calibrations. These limitations have encouraged the development of new reconstruction methods based on either biological or geochemical mechanisms.

The biological approach is still in its infancy, and it is derived from ecological studies of the requirements of the different species in the modern ocean. A first approach directly calibrates the proxies (foraminifera or others) from controlled laboratory cultures with varying physiological and geochemical constraints that duplicate those observed in the marine environment. A more theoretical approach complements these calibrations by modeling the growth conditions within the natural environment, using the experimentally calibrated variables. Using such methods, it may be possible to obtain a reliable reconstruction of the hydrology corresponding to the specific habitat of the different species of planktonic foraminifera (e.g., Lombard *et al.,* 2009).

21.2.2 Geochemical methods

21.2.2.1 Organic tracers

The organic geochemistry of marine sediments provides a different set of tracers. The most common so-called ‘biomarker’ is based on the changes in the abundance ratio of di- and tri- unsaturated alkenones (molecules with 37 carbon atoms containing two or three double bonds). This ratio is a function of the growth temperature of the synthesizing organisms, a group of algae called coccolithophorids, and in particular of the species *Emiliania huxleyi* for the modern ocean. The number of double bonds is inversely related to the temperature: the lower the temperature, the higher the number of double bonds (Prahl and Wakeham, 1987). The abundance ratio of di- and tri- unsaturated alkenones is conventionally expressed by the index $U^{k'}_{37}$:

$$U^{k'}_{37} = [C_{37:2}]/[C_{37:2} + C_{37:3}]$$

The initial calibration of the $U^{k'}_{37}$ index is based on *E. huxleyi* cultures in controlled conditions (Prahl and Wakeham, 1987) (Fig. 21.4), and has been subsequently verified using samples collected from ocean water or from the sediment surface (Müller *et al.*, 1998; Conte *et al.*, 2006; Tierney *et al.*, 2018).

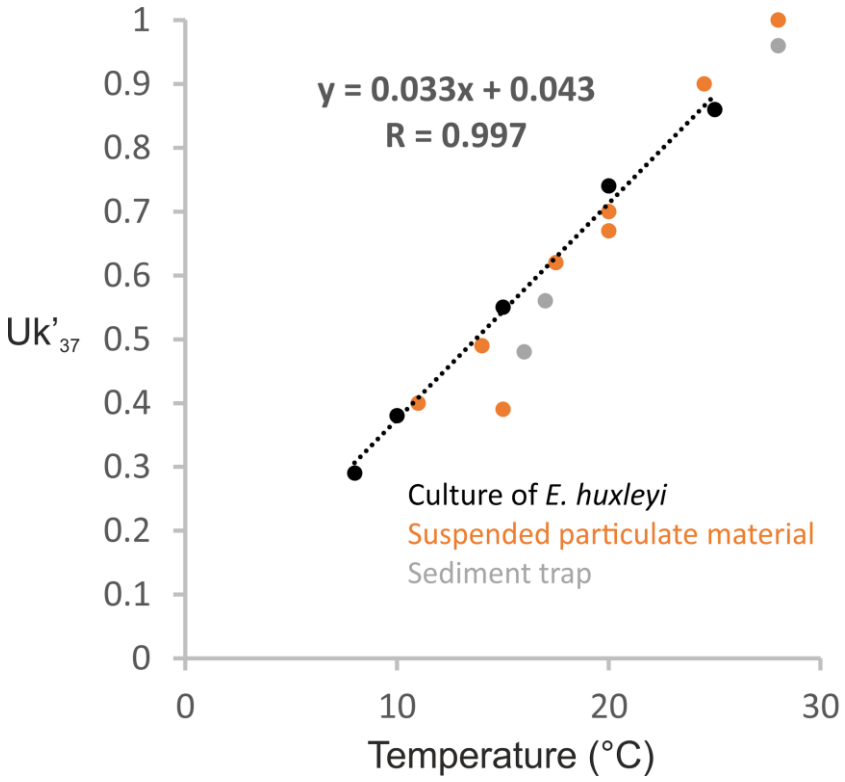

Fig. 21.4: Relationship between the unsaturation index $U_{37}^{k'}$ and SST. The line represents the temperature calibration curve based on cultures of *E. huxleyi* grown under laboratory conditions (Prahl and Wakeham, 1987). Natural particulate samples collected are indicated (Prahl and Wakeham, 1987).

However, like all paleoclimate indicators, the $U_{37}^{k'}$ index also presents various biases that limit its use in specific oceanographic contexts. A few of the most significant ones are as follows:

- The temporal evolution of the alkenone-producing species. *E. huxleyi*, which is currently the main producer of alkenones, was not present prior to MIS 8 (Thiersten *et al.*, 1977). Alkenones are also produced by other species such as *Gephyrocapsa oceanica*, but with different temperature - $U_{37}^{k'}$ index relationships. Care must therefore be taken when applying the $U_{37}^{k'}$ method to ancient sediments.

- The tiny coccolithophorids are easily transported by sea currents, so these algae can travel long distances between their place of production and place of sedimentation. A significant portion of the residual input to sediments may thus originate from remote areas with very different hydrological conditions. This problem is particularly significant in areas of low productivity or in frontal zones that separate two distinctly different water masses (Sicre *et al.*, 2005).

- Reconstructions could be biased toward a specific season (Rosell-Melé and Prahl, 2013) and a degree of nonlinearity may exist in the relation between alkenones and SST at the higher and lower ends of the temperature range (Conte *et al.*, 2006).

Another organic tracer to reconstruct past SST is based on the quantification of the average number of cyclopentane rings found in glycerol dialkyl glycerol tetraethers (GDGTs) of archaea membrane lipids. An index, called TEX_{86}, was deduced after analyzing the GDGTs distribution in marine surface sediments in comparison to annual mean SSTs (Schouten *et al.,* 2002).

Recently, a number of different TEX_{86} calibrations have been developed (Kim *et al.,* 2010; Tierney and Tingley, 2014; Ho and Laepple, 2016), in response to possible differences in membrane adaptation of the resident archaea communities at different temperatures, and to the differences found between the TEX_{86} ratio and other SST reconstruction proxies. A number of pre- and post-depositional processes can influence the TEX_{86} ratio. For some processes, this influence can be constrained. For example, the BIT index is used to track the amount of terrestrial GDGT input, using a ratio of branched versus isoprenoid GDGTs (Weijers *et al.,* 2006; Schouten *et al.,* 2013). Nonetheless, the scientific understanding of TEX_{86} remains imperfect, particularly since the effects of environmental factors such as salinity, nutrient concentrations, and water column structure may modulate the TEX_{86}–SST relationship (Tierney and Tingley, 2014).

21.2.2.2 Chemical tracers

The chemical composition of the carbonate from foraminiferal tests and coral skeletons may also provide paleotemperature or paleoenvironment indicators. For example, the concentration of magnesium incorporated in the calcium carbonate of foraminifera is an empirical function of the temperature at which that foraminifer crystallized its test. On time scales where the Mg/Ca of the oceans has remained constant, the sensitivity of Mg/Ca to temperature has been determined using either a culture-based, sediment trap or core top calibrations (see for example, Lea *et al.,* 1999; Elderfield and Ganssen, 2000; Anand *et al.,* 2003; Mashiotta *et al.,* 1999) (Fig. 211.5), and it takes the form:

$$Mg/Ca = B \exp(A*T)$$

Where A and B are the exponential and pre-exponential constants, respectively, and T is the temperature in °C.

Magnesium replaces calcium more easily at high than low temperatures, so the Mg/Ca ratio from carbonates increases with temperature at the time of calcite formation. Thermodynamic considerations suggested an exponential temperature dependence of Mg uptake into calcite (Rosenthal *et al.,* 1997).

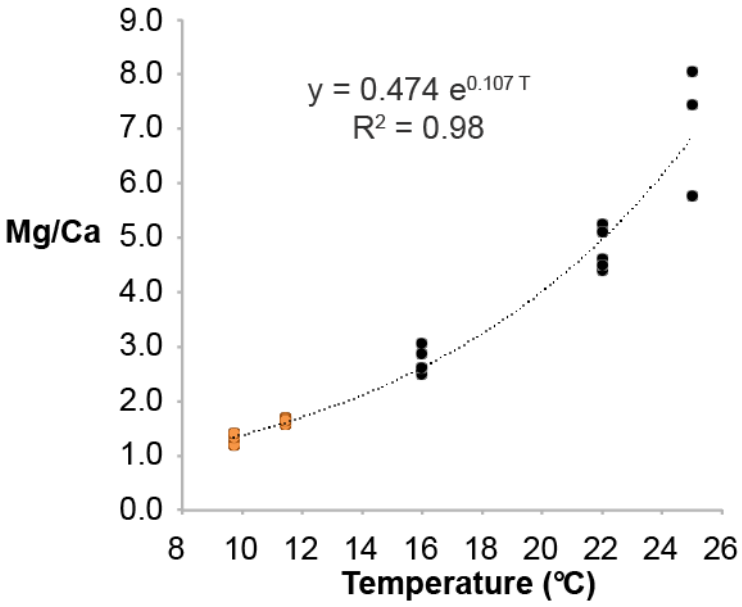

Fig. 21.5: Mg-temperature calibration results from culturing experiments with one species of planktonic foraminifera (*Globigerina bulloides*) (black dots) and core top samples (orange dots). Mg/Ca results are plotted versus calibration temperature (black dots) or World Ocean Atlas mean annual SST (orange dots) (modified from Mashiotta *et al.*, 1999).

However, the growth temperature is not the only factor to be considered. Seawater salinity and alkalinity have also been shown to significantly alter the Mg/Ca ratio in foraminiferal tests (Elderfield *et al.*, 2006; Mathien-Blard and Bassinot, 2009; Hönisch *et al.*, 2013). Another issue is the observed offsets in both culture and field studies between Mg/Ca ratios among individual species, that indicate the need for single-species calibrations. In addition, the geographical extension of genotypes must be assessed when choosing to develop calibrations (Vázquez Riveiros *et al.*, 2016). Recent studies try to simultaneously assess the relationship between foraminiferal Mg/Ca, and temperature, salinity, and the carbonate system using statistical approaches (Khider *et al.*, 2015; Gray *et al.*, 2018).

Mg/Ca in foraminifera has been cited here as a main example of a geochemical temperature tracer. Other ratios, such as Sr/Ca or Li/Mg in corals, are also used as tracers of temperature (Corrège, 2006; Montagna *et al.*, 2014).

21.2.2.3 Isotopic tracers

As presented in this chapter's introduction, the first isotopic approach developed was the relationship between temperature, the isotopic composition of seawater and the isotopic composition of the biocarbonate that developed within that water. Traditionally, isotopic compositions are expressed using the notation δ, which is the relative difference (expressed in parts per thousand) between the isotope ratio R of the sample and that of a reference standard:

$$\delta = [(R_{sample}/R_{st}) - 1] \times 1\,000$$

The $\delta^{18}O$ of the water is denoted δ_w, that of a carbonate, δ_c, and the relationship between temperature T, δ_w and δ_c is known as the ‘paleotemperature equation’. This relationship was

experimentally determined by Urey's group in the 1950s and improved by Shackleton (1974) in the form below:

$$T = 16.9 - 4.38 \times (\delta_c - \delta_w) + 0.10 \times (\delta_c - \delta_w)^2 \qquad (1)$$

In this empirical formula, δ_c represents the $\delta^{18}O$ of the CO_2 extracted from the carbonate through dissolution with phosphoric acid, and δ_w is the $\delta^{18}O$ of the CO_2 obtained by equilibration with the seawater to be analyzed. δ_c and δ_w are measured by mass spectrometry using the same CO_2 laboratory standard. Other $\delta^{18}O$ - temperature relationships defined in the last decades (Bemis *et al.*, 1998; Mulitza *et al.*, 2003; Marchitto *et al.*, 2014) use the same terminology.

Box 1

Practical application of the paleotemperature formula

Nowadays, isotopic geochemistry laboratories have adopted the convention of expressing the δ_c isotopic compositions against the PDB (Pee-Dee Belemnite) international standard and δ_w against the SMOW (Standard Mean Ocean Water) international standard. These standards are distributed by international agencies for laboratory calibration. To properly apply the paleotemperature formula, which presumes that all isotopic compositions are expressed relative to the same standard, it is necessary to compare the isotopic ratio of the CO_2 extracted from the PDB standard by controlled phosphoric acid attack with the isotopic ratio of the CO_2 isotopically equilibrated with the SMOW standard. The latter is lower in ^{18}O content by 0.27 ‰ than the CO_2 extracted from PDB, so that for every water sample:

$$\delta_w(vs.\ \text{PDB-}CO_2) = \delta_w(vs.\ \text{SMOW-}CO_2) - 0.27. \qquad (2)$$

If, as in the paleotemperature formula, PDB is used as the standard for carbonates and SMOW as the standard for waters, then Shackleton's equation becomes:

$$T = 16.9 - 4.38 \times (\delta_c - \delta_w + 0.27) + 0.10 \times (\delta_c - \delta_w + 0.27)^2.$$

One major disadvantage of the paleotemperature formula is that temperatures can only be determined if the isotopic composition of the water is known, which is almost never the case for geological samples.

A more recent isotopic method, still under development, is expected to overcome this constraint (Ghosh *et al.*, 2006; Schauble *et al.*, 2006). The crystal lattice of a carbonate consists of CO_3^{2-} groups and of cations (Ca^{2+}, for example). Among the CO_3^{2-} ions in a sample, the heavy isotopes ^{13}C and ^{18}O do not spread out randomly. Their relative abundance will depend on the isotopic equilibrium reaction:

$$^{13}C^{16}O_3^{2-} + {}^{12}C^{18}O^{16}O_2^{2-} \leftrightarrow {}^{13}C^{18}O^{16}O_2^{2-} + {}^{12}C^{16}O_3^{2-}$$

so that the distribution of these four isotopic species depends on their own binding energy, itself a function of temperature.

The abundance of the various isotopic species is assessed by dissolving the carbonate with phosphoric acid and measuring the abundance of $^{13}C^{18}O^{16}O$ molecules (with a mass of 47) in the extracted CO_2, and comparing this to the abundances of other isotopic species with masses 45 and 46. The 'stochastic' state is taken as a reference and is defined by a random distribution of the isotopes of C and O within the molecules.

The thermodynamic variable, denoted as Δ47, which describes the state of the carbon dioxide and from which we deduce a paleotemperature, is defined by the relationship:

$$\Delta 47 = [(R47/R^{*}47 - 1) - (R45/R^{*}45 - 1) - (R46/R^{*}46 - 1)] \times 1\,000$$

where *R*45, *R*46 and *R*47 are the abundance ratios of masses 45/44, 46/44 and 47/44, respectively, in the CO_2, and where *R**45, *R**46 and *R**47 denote these ratios for a gas with the same overall composition but in 'stochastic' state (Ghosh *et al.*, 2006).

The main advantage of this method (called the Δ47 method) is that the thermodynamic-measured value reflects an internal balance of the crystal lattice and requires no knowledge of the composition of the original water. This method is based on properties obeying thermodynamical principles, so it can be applied to a variety of environments without changes (Fig. 21.6).

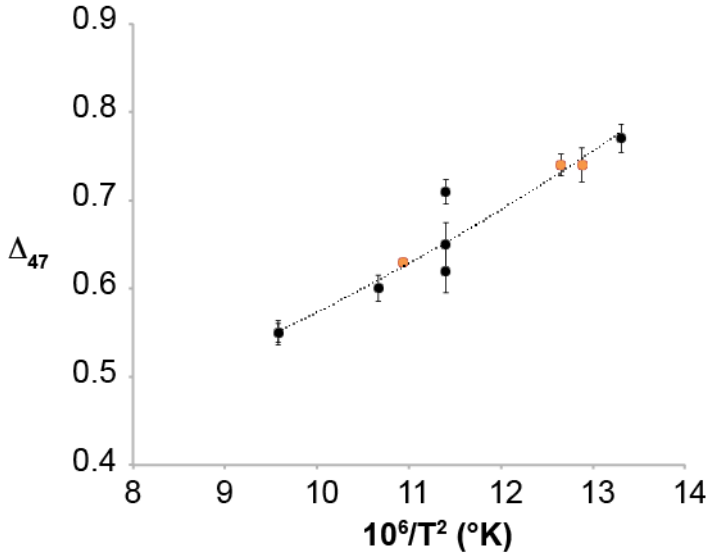

Fig. 21.6: Δ_{47} of CO_2 extracted from calcites grown from aqueous solution and of deep-sea corals (in orange) and surface corals (in black), plotted against $10^6/T^2$, where T is the known growth temperature in Kelvin (modified from Ghosh *et al.*, 2006).

However, as it is the case for the paleotemperature formula, the calibration performed by Ghosh *et al.*, (2006) only applies to carbonates precipitated at thermodynamic equilibrium. Therefore, testing for the possible existence of effects of parasitic isotopic fractionation of kinetic, biological or diagenetic origin should be carried out (Eiler *et al.*, 2014; Saenger *et al.*, 2012).

The temperature sensitivity of the Δ47 proxy is low (~0.003‰/°C) (Kele *et al.*, 2015). It

requires high measurement precision, which is commonly achieved by increasing counting times and/or the number of replicates analyzed per sample, a challenge for foraminifer-based reconstructions that use low carbonate samples. Recent studies have focused on the development of precise standardized calibrations that are applicable to paleoceanographic studies (Peral *et al.*, 2018).

21.3 Sea surface salinity

While the temperature of seawater varies over a range of more than 30 °C in the open ocean, salinity changes much less (between 33 and 38 g of salt per liter (psu)). Salinity is highest in tropical areas, where evaporation exceeds precipitation (Fig. 21.7), and it decreases where precipitation dominates, in the equatorial belt and at high latitudes. As the hydrological cycle is greatly affected by the glaciations, significant variations in the salinity of the ocean during the Quaternary are to be expected.

Temperature and salinity jointly determine the density of seawater, the driver of deep ocean circulation. Dense waters sink at high latitudes and are progressively redistributed by deep currents through the various basins of the world's oceans. The reconstruction of the distribution of surface water salinity in the past would thus contribute to the understanding of why and how ocean circulation changed when climate conditions were different from today. It will also provide modelers with quantitative estimates to use as a forcing of numerical climate models.

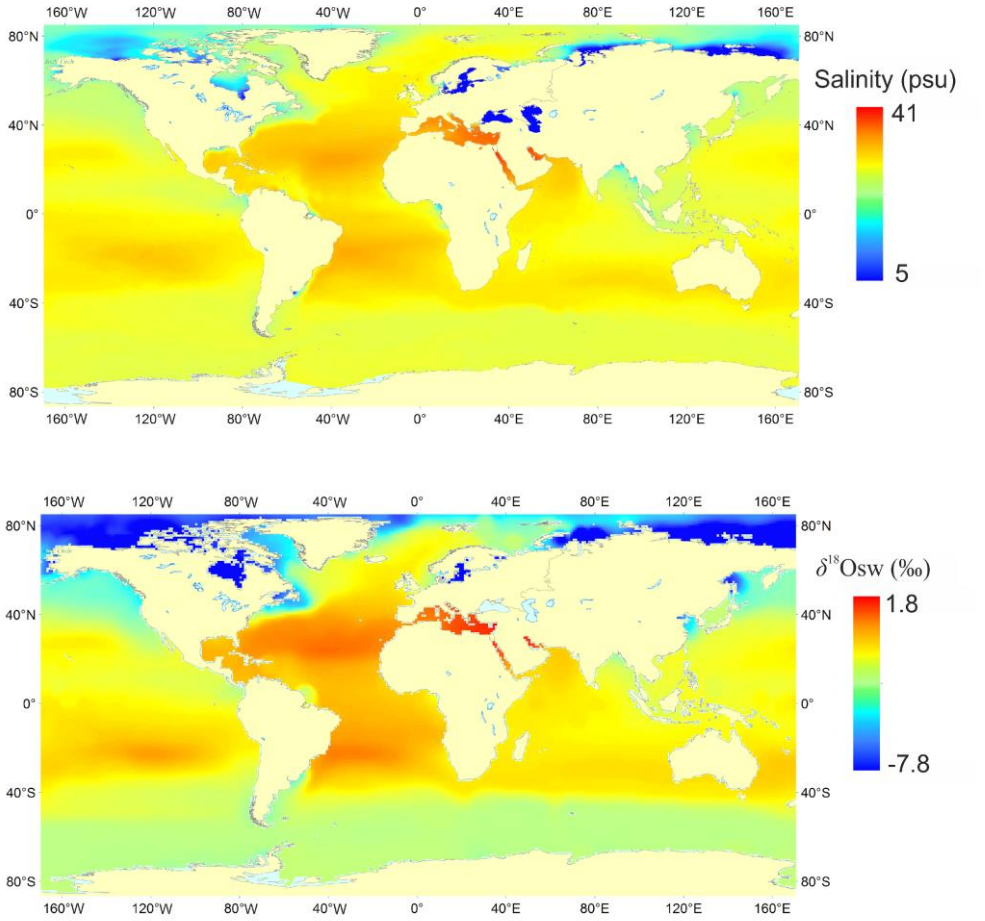

Fig. 21.7 – Surface salinity of the modern oceans (WOA 2013, Zweng *et al.*, 2013) and gridded data set of surface $\delta^{18}O$ of seawater (δ_w) (Legrande and Schmidt, 2006).

Estimating the surface water salinity distribution of past oceans is difficult, partly due to the close correlation of temperature and salinity. Because of this correlation, changes in plankton distribution and transfer functions do not differentiate between changes in SST and changes in salinity. Moreover, the dominant signal recorded by most indicators is often temperature.

Nonetheless, reconstructions of past sea surface salinity (SSS) using transfer functions of dinoflagellate or diatom assemblages have been proposed in specific marine environments (DeSève, 1999; De Vernal *et al.*, 2001) with an accuracy of ±1.8 psu for the present day (De Vernal *et al.*, 2001). However, these methods are difficult to extrapolate unambiguously to a global scale due to non-analogue situations in the past.

The most common method presently used to reconstruct past SSS is the calibration of salinity against stable oxygen isotope ratios measured on foraminifera (Duplessy *et al.*, 1991; Malaizé and Caley, 2009). Geochemical methods based on the analysis of trace metals have recently been developed; we will briefly discuss these two approaches in the sections that follow.

21.3.1. Isotopic methods

21.3.1.2 Paleosalinities from stable oxygen isotopes ($\delta^{18}O$)

In the open ocean, the isotopic composition of seawater is closely correlated to salinity (Figs. 21.7 and 21.8): the vapor pressure of $H_2{}^{18}O$ being lower than that of $H_2{}^{16}O$, isotopic ratio of vapor in the atmosphere is systematically lower than in the condensed phase (ocean and rain). The more evaporation exceeds precipitation, the higher the surface water isotopic ratio. At local to regional scale, there is a linear relationship between salinity and δ_w (Fig. 21.8). This is the relationship which allows the estimation of past seawater salinities.

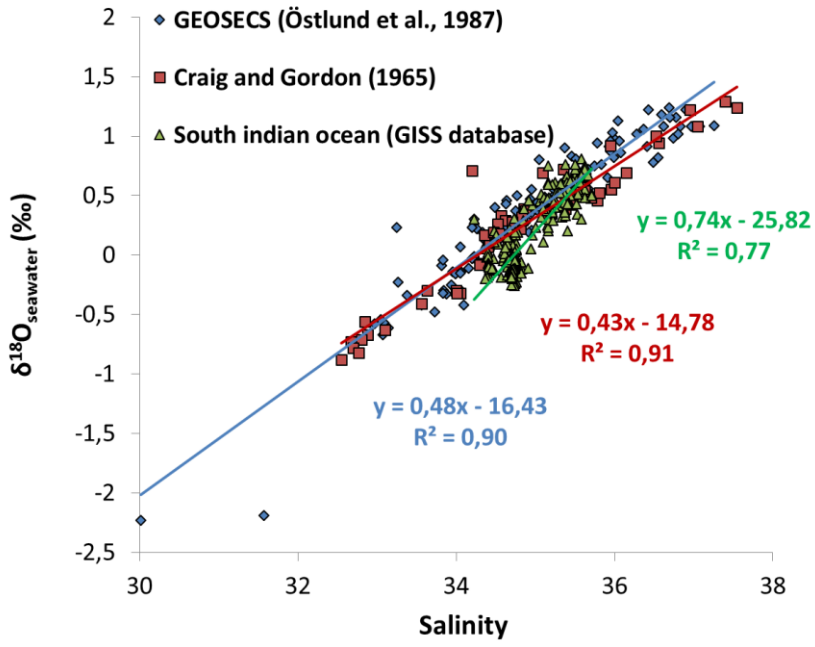

Fig. 21.8 – The relationship between surface δ_w and salinity for the global ocean as measured within the international GEOSECS program (Ostlund *et al.*, 1987), by Craig and Gordon (1965), and for the South Indian Ocean with the GISS database (Schmidt *et al.*, 1999).

The major uncertainty in the 'paleotemperature formula' now becomes an advantage. δ_w can be determined when δ_c is measured if the foraminiferal habitat temperature T is estimated independently (by Mg/Ca ratios analysis of the same shells for example).

In the past, δ_w has been seen to vary globally. When the ice caps grew on land, they trapped snow poor in ^{18}O, and so the δ_w of the ocean increased. Thus, we observe a simultaneous drop in sea level and an increase in δ_w. Conversely, when the ice caps melt, sea level rises and δ_w decreases. The most recent studies (see Chapter 2, Volume 2) estimate that sea level dropped by about 120 meters during the LGM, and that the average isotopic composition of the ocean was then at +1.0 ‰ SMOW (while the current value is 0‰ SMOW by definition). Various approaches aim to reconstruct changes in sea level linked with changes in continental ice volume. It is then feasible to estimate the change in mean ocean δ_w

related to variations in continental ice volume and sea level.

Locally, changes in the hydrological cycle (evaporation, precipitation, water mass movements, melting events) can cause additional variations in δ_w, of both climatic and hydrological origin.

Reconstructing the evolution of the isotopic composition of seawater in the past is in itself a challenging task because δ_w tracks changes in the hydrologic cycle. However, we can try to qualitatively interpret a record of paleo δ_w in terms of paleosalinities (see Box 2).

Box 2
Practical calculation of paleosalinities

Estimating paleosalinity changes along a sediment core requires the following steps:

- Measure δ_c and T at each level so as to derive a recording of paleo δ_w over the time period covered by the core, using the paleotemperature equation (equation 1);

- Estimate global δ_w changes (δ_w^{ice}) related to continental ice volume variations over the study period using known records of changes in sea level. A drop of 120 meters in sea level is accompanied by an increase in δ_w^{ice} of +1.0 ‰. Given an average depth of the modern ocean of ~3900 meters and an average salinity of 34.7 psu, and since the amount of salt in the ocean remains constant, a drop in sea level of 120 meters is also accompanied by an increase in salinity. The average ocean salinity becomes:

$$(34.7 \times 3900) / 3780 = 35.8 \text{ psu.}$$

  Salinity has thus increased by about 1.1 psu and δ_w^{ice} by +1.0‰. Coupled models of the Northern Hemisphere ice sheets allow the ice-sheet contribution to the variability in oxygen isotope composition and sea level changes to be determined (Bintanja *et al.,* 2005).

- Estimate the variation in local isotopic composition δ_w^{local} due to hydrological changes by subtracting δ_w^{ice} changes from the δ_w value reconstructed for each core level. The corresponding change in salinity can be estimated from current observations (Fig. 21.7).

The statistical error associated with this approach is high and rarely permits meaningful quantitative salinity reconstructions because of the associated large uncertainties (Rohling and Bigg, 1998; Schmidt, 1999; Rohling, 2000; Legrande and Schmidt, 2011; Caley and Roche, 2015). The structural/analytical error is in the range of 0.8–1.8 psu (Schmidt, 1999). In addition, the spatial and temporal evolution of the slope of the δ_w-salinity relationship, tested in isotope-enabled numerical climate models, can lead to very large errors (Legrande and Schmidt, 2011), up to 25 psu in certain regions for the LGM (Caley and Roche, 2015).

To reduce these very large errors on past SSS reconstructions, model-derived temporal slopes of the δ_w-salinity relationship can be used directly in the calculation. This approach has been tested with success for the LGM on a marine sediment record located in Gulf of Guinea and influenced by West African monsoon hydrology (Caley and Roche, 2015). However, allowing model-derived regional δ_w-salinity relationships to vary through time can lead to significant uncertainties related to the shortcomings of the models, so complementary approaches should also be developed.

21.3.1.2 Paleosalinities from stable hydrogen isotopes (δ^2H)

Another method uses hydrogen isotope changes to reconstruct paleosalinities. Culture experiments have found a constant offset between the hydrogen isotopic composition of water and the hydrogen isotopic composition of alkenones synthesized in that water (Paul, 2002; Englebrecht and Sachs, 2005). Schouten *et al.,* (2006) demonstrated that this offset was dependent on salinity via biological fractionation processes. Reconstructing salinity by using the biological fractionation factor that is linked to it requires information on the past hydrogen isotope ratio of seawater (δ^2H_w).

Isotope-enabled climate model results indicate a rather stable dependence between δ^2H and surface δ_w in the past (Caley and Roche, 2015). As δ_w can be reconstructed (see section 21.3.2) this suggest that δ^2H_w can also be obtained. An estimation of paleosalinities based on δ^2H measurements in alkenones might therefore be possible if the slope and the intercept of the regression between the biological fractionation factor and salinity can be sufficiently constrained. The impact of species composition and growth phase on the use of alkenone δ^2H to reconstruct paleosalinity currently requires further investigations (Wolhowe *et al.,* 2009; Chivall *et al.,* 2014; M'Boule *et al.,* 2014).

Pairing information from water isotopes, $\delta^{18}O$ and δ^2H (isotopologues), could yield better estimates for paleosalinity (Rohling, 2007; Leduc *et al.,* 2013). Numerical modeling experiments for the Holocene and the LGM periods have demonstrated that this combination of water isotopologues may indeed allow for a better estimation of paleosalinity variability (Legrande and Schmidt, 2011; Caley and Roche, 2015). Nonetheless, ecological biases introduced by combining proxies based on two different organisms (foraminifera are zooplankton and coccoliths are phytoplankton) could emerge, together with differences in dissolution and bioturbation in a sediment core.

21.3.2 Chemical methods

Calibrations established using the modern Ba/Ca-salinity relationship (Carroll *et al.,* 1993; Weldeab *et al.,* 2007) (Fig. 21.9) have suggested that the Ba/Ca ratio of foraminiferal $CaCO_3$ can be used as a proxy for river runoff. This approach is limited to coastal regions affected by river runoff (i.e. prone to relatively large salinity changes) and assumes that (1) the Ba/Ca ratio in planktonic foraminifera shells is dominated by the Ba/Ca concentration of seawater (Hönisch *et al.,* 2011) and not by other factors and (2) that the present-day calibration is applicable to the past.

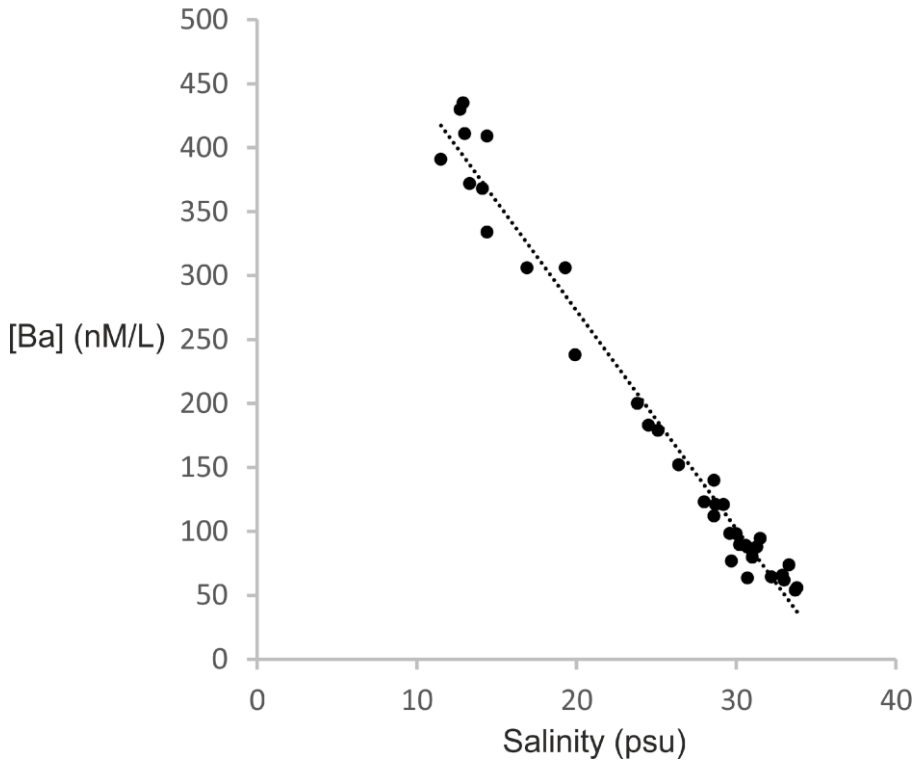

Fig. 21.9: Relationship between Ba in seawater and salinity in the Bay of Bengal (Carroll *et al.*, 1993).

Another recent study has established the potential of the Na/Ca ratio of foraminiferal calcite as a quantitative proxy for past salinities. In culture experiments, Wit et al., (2013) studied sodium incorporation in the benthic foraminifera *Ammonia tepida* at a range of salinities and suggested that foraminiferal Na/Ca could serve as a robust and independent proxy for salinity. More recently, the field study of Mezger *et al.*, (2016) on planktonic foraminifera also suggested that salinity controls foraminiferal Na/Ca. Incorporation of Na in foraminiferal calcite could therefore constitute a potential proxy for salinity, although species-specific calibrations are still required and more research on the effect of temperature is needed.

21.4 Reconstruction of the hydrology of the deep ocean

21.4.1 Main features of modern circulation

On a rotating planet like the Earth, surface ocean circulation is governed by the winds and the position of the continents that define the shape of the ocean basins. Deep circulation, on the other hand, is governed by the small variations in the density of the water masses. Since density depends on temperature and salinity, the term ‘thermohaline circulation’ is used. Reconstructing past changes in temperature, salinity and density in the intermediate and deep ocean is thus needed to understand the temporal variations of the circulation and distribution of water masses; it also provides a benchmark for simulations provided by general circulation models.

As we saw in Chapter 1, deep waters are currently formed in winter in highly localized areas of the high latitudes: the Norwegian Sea and the Labrador Sea in the northern hemisphere and the Weddell Sea and the Ross Sea near Antarctica. During winter, surface waters here become denser as they cool down but also because the formation of sea ice is accompanied by a release of salt. When surface waters become as dense as deep waters, large-scale convection movements are initiated and the waters sink into the abyssal depths. Once at depth, very small changes in density of the various deepwater masses govern their circulation through the different basins. Surface waters sinking in the Norwegian Sea cross the sills separating it from the Atlantic Ocean to form North Atlantic Deep Water (often referred to by the acronym NADW). This water mass then follows the American coast to join the Southern Ocean and is caught up in the Antarctic divergence, a large upwelling zone, where it mixes with the surface waters of southern high latitudes. Here, these very cold surface waters increase their density through winter sea ice formation, and sink along the Antarctic continental shelf forming the densest waters in the world. This water mass is called Antarctic Bottom Water (or AABW), and it lines the bottom of all ocean basins. At present, abyssal waters are not formed from the surface waters of the Indian and Pacific Oceans. The Antarctic waters that rush into these basins create the Pacific and Indian Deep Waters (PDW and IDW, respectively) by mixing with the waters of the main thermocline, and then return to the Southern Ocean at around 3 km depth. We can devise a simplified view of the global ocean circulation, where the Norwegian Sea is the main source of deep waters, and the Southern Ocean acts as a recirculation pump returning to the depths the surface waters surrounding Antarctica that have received upwelled NADW via the Antarctic divergence. This circulation pattern is critically dependent on the climate of the high latitudes of the Northern Hemisphere (North Atlantic Ocean, Norwegian and Labrador Seas) and of the Southern Ocean in the Southern Hemisphere.

21.4.2 Reconstructing the temperature and salinity of deep waters

The past evolution of the deep ocean has been the subject of extensive research. However, the reconstruction of the basic properties of bottom waters has been hindered by the lack of transfer functions linking the abundance of benthic species to the temperature of seawater in the vicinity of the sediment. In many environments, these abundances are essentially governed by the availability of food and by the proportion of dissolved oxygen. However, paleoceanographers have attempted to apply other approaches to the reconstruction of bottom water temperature.

21.4.2.1 Searching for a reference zone with constant temperature

As early as 1967, Shackleton (1967) suggested that the $\delta^{18}O$ of benthic foraminifera must closely resemble the $\delta^{18}O$ of deep waters, because these waters are formed close to freezing conditions and their temperature cannot drop much further during a glacial period. Labeyrie *et al.*, (1987) further elaborated on this concept by analyzing the $\delta^{18}O$ of benthic foraminifera from a core in the Norwegian Sea where temperature, well below 0 °C in the deep basins, is constrained by exchanges with the ice. By comparing the isotopic record from this core with others from the Pacific and Indian Oceans, the authors were able to demonstrate, contrary to

the assumptions of Shackleton, that deep water temperature in the major ocean basins did change significantly at the beginning of the last glaciation, with a cooling in all deep oceans to a temperature close to the freezing point (∼-1 °C) during the LGM. This result has been confirmed since by other tracers such as the Mg/Ca ratio of benthic foraminifera (see section 21.4.2.2). Unfortunately, the isotopic benthic record of the Norwegian Sea is far from continuous and this method could not be successfully applied to reconstruct the evolution of the abyssal water temperature over the whole of the Quaternary

It should be emphasized, however, that very low deep-water temperatures during glacial periods are to be expected. Indeed, under current conditions, NADW is formed from very cold water (close to the freezing point) that overflows from the Norwegian Sea through the sills located between Scotland, the Faroe Islands, Iceland and Greenland. However, the water that crosses these shallow sills (with a depth of less than one kilometer) mixes with the much warmer waters of the North Atlantic, so that the newly formed NADW is characterized by a temperature of +3°C and a salinity of 34.95 psu. Its density remains high, close to but slightly less than that of AABW (temperature of -1 to 0 °C, salinity of 34.6 psu). It is therefore AABW that lines the great ocean depths, and, in the Atlantic Ocean, is topped by NADW. During the last glaciation, the sinking of very cold water directly into the North Atlantic (and not into the Norwegian Sea anymore) explains why the deep waters of the world are all found to be at temperatures close to the freezing point.

21.4.2.2 Estimating the temperature independently of the paleotemperature formula

The simplest way to determine the temperature of the water close to the sediment is to use the concentration of trace metals (Mg/Ca) contained in the carbonate shells of benthic foraminifera. This independent estimate of bottom water temperature allows the calculation of the δ_w of deep water using the paleotemperature formula.

However, the temperature dependence of Mg incorporation in benthic foraminiferal tests is species-specific, and may depend on different hydrological factors such as salinity or carbonate ion saturation (Elderfield *et al.*, 2006). In addition, the expected bottom water temperature variations during glacial-interglacial cycles are small compared to surface temperature changes, implying relatively small Mg/Ca variations. The recently discovered $\Delta 47$ method is only starting to be applied to this problem (Peral *et al.*, 2018), although more precise measurements in benthic foraminifera are needed to confirm the utility of this technique.

21.4.2.3 Searching for the geochemical signature of ancient waters in pore waters

Adkins *et al.*, (2002) found that in long cores extracted by drilling ships, pore water trapped within the sediments shows measurable differences in salinity and in δ_w. These differences increase initially with core depth, then reach a maximum after which they decrease slowly. They interpreted this maximum as the signature of highly saline water from the LGM that had diffused into the sedimentary column. Using a simple diffusion model, the authors estimated the values for the salinity and the δ_w of the bottom waters 20 ka ago. Using this estimate of the δ_w of bottom waters, and combining it with $\delta^{18}O$ measurements on the

calcite of benthic foraminifera, the paleotemperature formula confirmed that the deep waters of the glacial ocean were actually at a temperature near freezing point and hypersaline. The sediment cores that have been measured for δ_w are too few to give a complete picture of the ocean during the last glaciation. However, they show a significant disparity in the salinities from one basin to another, with the Southern Ocean being the saltiest, in contrast with the modern situation.

21.4.2.4 Reconstructing changes in water mass distribution

Lynch-Stieglitz *et al.,* (1999) and (2014) showed that an approximate direct relationship could be established between the $\delta^{18}O$ of benthic foraminifera and the density of seawater, within the temperature range where the temperature-salinity-density relationship is roughly linear (*T* greater than 2 °C). In this way, the authors were able to study the geostrophic deformations of the deep thermocline in the Straits of Florida and propose estimates of the changes in the meridian flow linked to the Atlantic thermohaline circulation between the LGM and the present.

Reconstructions using benthic foraminiferal $\delta^{18}O$ have also shown marked changes in the distribution of deep and intermediate water masses during the LGM compared to the present day. In the Atlantic Ocean, the temperature gradient currently observed at the base of NADW at around 3000 m was to be found at around 2000 m, and was much more pronounced than the one that currently separates NADW and AABW (Labeyrie *et al.,* 1992). In the Indian Ocean, a strong gradient separated two water masses with distinctly different characteristics at a depth of around 2000 m (Kallel *et al.,* 1988). More recent research even suggests the presence of a third deep water mass in the deepest North Atlantic at the LGM, formed by brine rejection and not by heat loss to the atmosphere (Keigwin & Swift, 2017).

21.4.3 Reconstructing the circulation of deep waters

21.4.3.1 Searching for lines of current from the $\delta^{13}C$ of benthic foraminifera

An original approach, independent of temperature and salinity, tries to characterize the main features of deep water circulation without trying to *a priori* understand the underlying physical mechanisms governing it. It is based on the carbon cycle and its tracer, the $^{13}C/^{12}C$ ratio usually denoted as $\delta^{13}C$. At the ocean surface, waters easily exchange their gas content with the atmosphere; they contain carbon dioxide and are rich in dissolved oxygen. During photosynthesis, phytoplankton preferentially absorbs $^{12}CO_2$ over $^{13}CO_2$. The organic material thus produced has a $\delta^{13}C$ close to −20 ‰, while the $\delta^{13}C$ of dissolved CO_2 in surface waters varies between +1 and +2 ‰. This surface organic matter forms the base of the ocean's food chain, and eventually falls to the depths carried in fecal pellets of zooplankton and higher animals. In the water column, settling organic matter undergoes a slow remineralization, which consumes any dissolved oxygen that may remain and produces CO_2 depleted in ^{13}C. Consumption of dissolved oxygen and production of CO_2, accompanied by a decrease in $\delta^{13}C$, take place in the deep waters (Fig. 21.10). The $\delta^{13}C$ of dissolved CO_2 in deep waters is thus lower than that of the surface waters.

The remineralization of organic matter is a slow process. This is why deep waters are characterized by a high $\delta^{13}C$ in regions close to their formation area (this is the case for the North Atlantic Ocean). Gradually, as they move away and circulate at depth, without the opportunity to exchange with the atmosphere, they become increasingly deprived of dissolved oxygen, while their $\delta^{13}C$ decreases through the mechanism described above. To give an order of magnitude, we can consider that the $\delta^{13}C$ of deep water decreases by about 1 ‰ per thousand years.

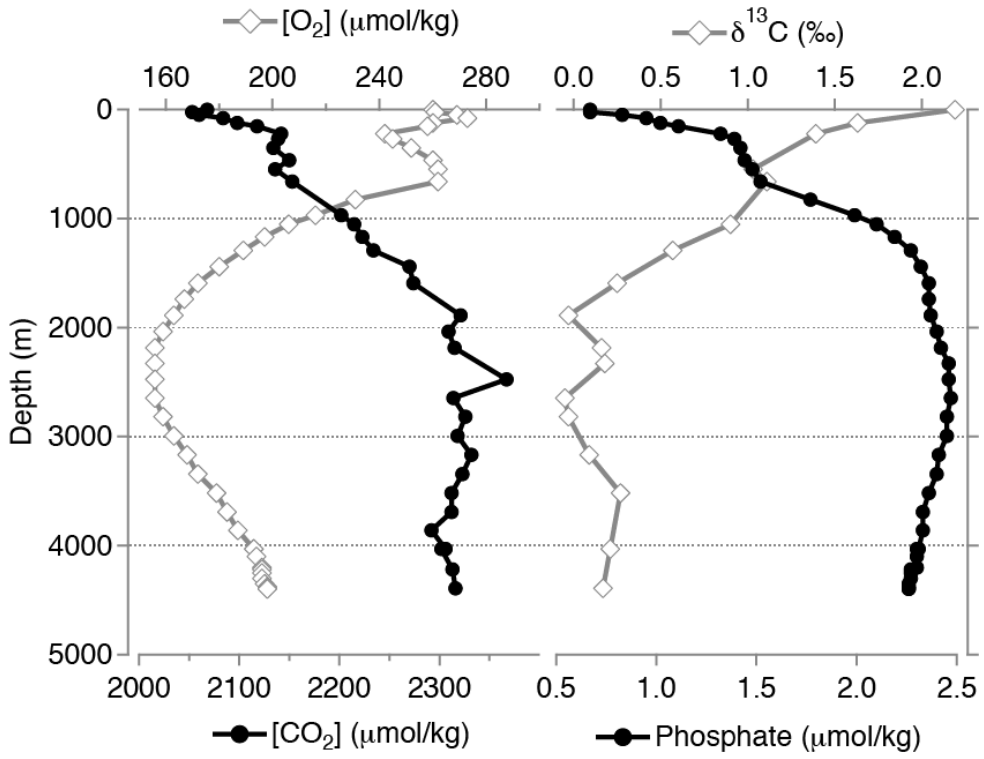

Fig. 21.10 – Variations in the concentration of dissolved oxygen, the concentration of total dissolved CO_2, the $^{13}C/^{12}C$ ratio of the total dissolved CO_2 and phosphate with respect to depth at GEOSECS station 322 in the Pacific Ocean (43.0°S / 129.9°W). The oxygen minimum at depth indicates consumption by marine bacteria. The resulting CO_2 production is characterized by a maximum of dissolved inorganic carbon concentrations and by a minimum of $\delta^{13}C$ (since carbon in organic matter is depleted by about 20 ‰ relative to dissolved inorganic carbon).

It is therefore the waters of the deep basins of the Pacific and Indian Oceans, at the end of the circulation scheme described in section 21.4.1, which have the lowest $\delta^{13}C$. The evolution of $\delta^{13}C$ in the deep ocean can thus be used as a tracer to characterize the lines of current and the exchanges between the various deep water masses. Epibenthic foraminifera, such as the species *Cibicides wuellerstorfi*, reflect this evolution of the water in which they grew, and variations in their $\delta^{13}C$ in cores extracted from different ocean basins are used to reconstruct changes in ocean circulation through time (Duplessy *et al.*, 1984; Schmittner *et al.*, 2017). For example, this proxy has been used to reconstruct ocean circulation during the LGM, when well ventilated (with a high $\delta^{13}C$) waters of the Atlantic Ocean formed Glacial North Atlantic Intermediate Waters (GNAIW), at a shallower depth than today's NADW, while deep waters (AABW) were even more poorly ventilated than today (Fig. 21.11). The understanding of this

variability in the thermohaline circulation, which is a major regulatory mechanism of climate, is the subject of substantial research, both analytical and in modeling.

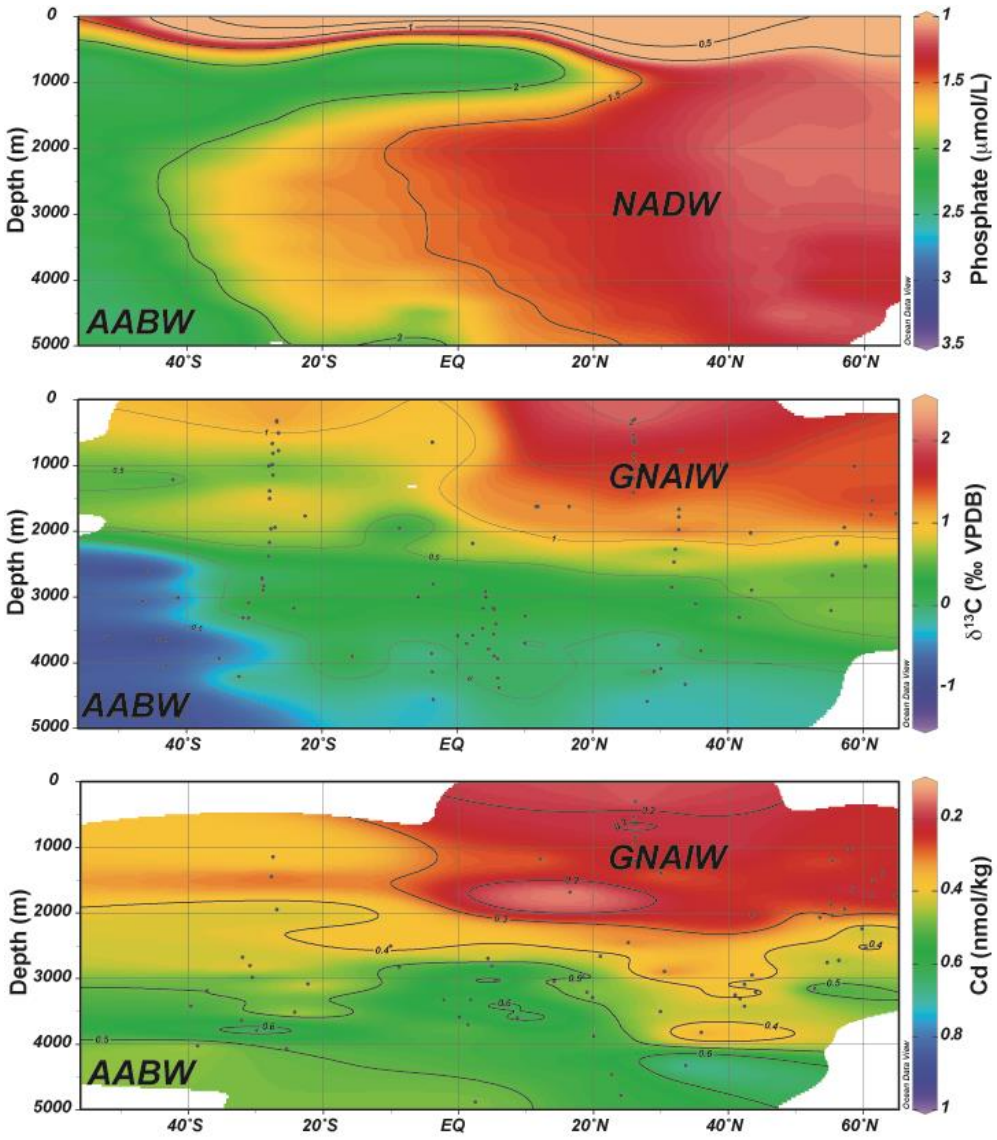

Fig. 21.11 – (Top) Modern distribution of dissolved phosphate (µmol/liter) in the western Atlantic; (middle) reconstructed benthic $\delta^{13}C$ in the western and central Atlantic during the LGM; (bottom) estimates of the Cd concentration (nmol/kg) during the LGM based on the ratio of Cd/Ca in the shells of benthic foraminifera (figure modified from Lynch-Stieglitz *et al.*, 2007).

21.4.3.2 Using trace elements measured in benthic foraminifera

In the modern ocean, geochemists have showed that cadmium (Cd) is included in organic matter, so that its cycle follows that of phosphate. The concentration of dissolved Cd in ocean waters shows therefore very similar variations to that of dissolved phosphate, a nutrient with a well-known cycle. It is assimilated by phytoplankton to ensure growth, so, as for all organic matter formed by photosynthesis, it falls into the water column with organic debris and is gradually released in the deep waters as bacteria oxidize it. Consequently, in the deep waters of the ocean, the consumption of dissolved oxygen and production of carbon dioxide

(depleted in ^{13}C as we have seen) occur in parallel with increases in phosphate and cadmium.

The Cd ion has a charge and an ionic radius similar to that of Ca. It is therefore easily incorporated in trace amounts into the carbonate shells of benthic foraminifera, so that their Cd/Ca ratio reflects the concentration of Cd in the seawater in which the foraminifera developed. The Cd/Ca ratio is therefore a tracer for nutrient concentration of the water masses, present and past (Marchitto & Broecker, 2006; Figure 21.11).

Cd and ^{13}C have similar geochemical behaviors, with the essential difference that surface waters can exchange their dissolved carbon dioxide with the atmosphere, while Cd is not involved in ocean-atmosphere exchanges. In general, there is an excellent anti-correlation between the variations in the Cd/Ca ratio and the $^{13}C/^{12}C$ of benthic foraminifera measured in sediment cores. One notable exception is the Southern Ocean, where the benthic foraminifera that lived during the last ice age have very negative $\delta^{13}C$, while their concentrations in Cd are very similar to those of recent sediments from the Holocene. Despite inter-specific differences that may have affected $\delta^{13}C$ reconstructions based on benthic foraminifera (Gottschalk *et al.*, 2016), or diagenetic and metabolic effects influencing the incorporation of trace metals into biogenic calcite (Marchitto & Broecker, 2006; McCorkle *et al.*, 1995), this discrepancy between the two indicators remains still to be explained.

21.4.3.3 Reconstructing the dynamics of water masses

The tracers we have described so far allow the reconstruction of specific physical or chemical characteristics of water masses, but they do not convey information on their dynamics. In this section, we do not discuss in detail tracers related to particle transport at the ocean floor (particle size distribution, magnetic grain size, sortable silt). However, we will discuss two unstable radioactive tracers in the ocean: the concentration in ^{14}C of benthic foraminifera and the excess $^{231}Pa/^{230}Th$ ratio in sediments.

When surface waters exchange carbon dioxide with the atmosphere, they absorb ^{14}C. Currently, the ^{14}C concentration in the surface ocean is 95% of that of the atmosphere. When surface waters sink, they bring with them the dissolved carbon dioxide as well as the ^{14}C they contain. Once they reach the bottom of the ocean, these waters are isolated from the atmosphere, and ^{14}C decreases due to its own radioactive decay, with its period of 5720 years. The oldest waters in the northern Pacific and Indian Oceans have an apparent age of around 800 years (see Chapter 4). The planktonic foraminifera (that live in surface waters) and the benthic foraminifera (that live on the ocean floor) incorporate the ^{14}C of the waters around them into their shells. By comparing, at the same level of sediment, the ^{14}C ages of planktonic and benthic foraminifera, we can estimate the apparent age of the deep waters over the last ~ 40,000 years. This apparently simple method presents in fact many difficulties. Firstly, despite recent analytical developments, benthic foraminifera are not always sufficiently abundant, and it may be difficult to obtain the amount of carbonate required for analysis from a normal-size sample, even using the most sensitive technique, accelerator mass spectrometry. Second, the ^{14}C ages of foraminifera, once in the sediment, are very sensitive to bioturbation: the abundance of one species shows considerable variation over time, and shells that are

found at one level may have been displaced by the activity of burrowing animals and therefore come from a significantly different age level than the selected one (Chapter 4). Finally, the atmospheric ^{14}C concentration has undergone large scale changes, so much so that the difference in ^{14}C age between planktonic and benthic foraminifera does not directly reflect the residence time of the waters at depth.

Another approach to reconstruct the dynamics of deep-water masses makes use of the geochemical behavior of the decay chain of uranium in seawater. The isotopic composition of dissolved uranium is constant throughout the ocean. Two of the isotopes of uranium, ^{235}U and ^{234}U, decay producing ^{231}Pa and ^{230}Th respectively, with an output ratio that is constant and equal to 0.093. ^{231}Pa and ^{230}Th are very reactive to particles sinking in the water column: they are adsorbed on their surface and settle as sediment along with them. However, ^{231}Pa is less reactive than ^{230}Th, so that the residence time in seawater of dissolved ^{231}Pa is close to 200 years, while that of dissolved ^{230}Th is only thirty years (Yu *et al.,* 1996). The residence time of ^{231}Pa is close to that of NADW in the Atlantic. Because of this, a fraction of the dissolved ^{231}Pa is advected out of the North Atlantic Ocean by NADW (about 50% in the modern ocean), while ^{230}Th is unaffected and settles completely with the particles. The net loss of ^{231}Pa in the water column at depths greater than or equal to the level at which NADW flows, leads to a deficit of ^{231}Pa in the sediments and therefore in the $^{231}Pa/^{230}Th$ ratios below the production ratio (0.093). If the circulation of NADW becomes slower, less ^{231}Pa is advected out of the basin, and the $^{231}Pa/^{230}Th$ ratio of the particles settling to the sediment increases to values closer to the production ratio.

It should be noted that sediments also contain ^{231}Pa and ^{230}Th, present as daughter isotopes of the uranium in clays that have reached secular equilibrium with their relevant parents. The addition of ^{231}Pa and ^{230}Th from settling particles thus produces an excess of these two radioisotopes in the sediment. Measuring the ratio of excess $^{231}Pa/^{230}Th$ in the sediments therefore allows the variations in the circulation of deep waters from the North Atlantic towards the Southern Ocean to be traced, and so to detect the variability associated with major changes in climate (McManus *et al.,* 2004; Gherardi *et al.,* 2009; Lippold *et al.,* 2016). This technique has been used with success to reconstruct the ‘strength’ of the thermohaline circulation back to ~ 140 ky ago (Guihou *et al.,* 2010; 2011; Böhm *et al.,* 2015).

21.5 Major fields of paleoceanography

A prerequisite to reconstruct ocean circulation in the past is that marine sediments have not been buried in the mantle at subduction zones. Due to the renewal of the ocean floor by plate tectonics, the oldest sediments date back to the Triassic, about 200 million years ago. These very old sediments are rare, and found only in the Pacific Ocean. In practice, we can hope to obtain global reconstructions for the whole Tertiary era, but they become increasingly scarce as we go back to the Secondary era. Here, we will restrict ourselves to the analysis of some of the major aspects of the evolution of climate and paleoceanography over the last 25 million years, which correspond to the progressive establishment of glacial conditions in the high latitudes of both hemispheres.

21.5.1 From ‘the greenhouse effect era’ to the ‘ice ages’

The Quaternary period, which covers the last 2.6 million years of the history of our planet, is characterized by persistent major ice sheets in the high latitudes of both hemispheres. The volume of these caps and their geographical expansion fluctuate over timescales of 10^4 to 10^5 years, in response to changes in insolation controlled by the orbital parameters of the Earth (see Chapter 7, Volume 2).

The origin of these major glacial phases is discussed in several chapters that present the point of view of geophysicists, geochemists and modelers (see Chapters 2, 5 and 6, Volume 2). At time scales exceeding a million years, the major causes of the development of glaciations are feedbacks related to plate tectonics. Among these feedbacks, the following may be highlighted:

– the varying shapes and positions of landmasses and ocean basins,

– the existence of passages between basins,

– the location and altitude of mountain ranges, both in the ocean and on land, affecting oceanic and atmospheric circulation and heat transfer,

– volcanism and erosion, and their impact on atmospheric chemistry and on the pCO_2 of the atmosphere.

The record describing the evolution of the $\delta^{18}O$ of benthic foraminifera over time shown in Figure 21.2 is the result of a compilation of analyses made in more than forty ocean-drilling sites. This global compilation registers both the changes in δ_w and temperature, in accordance with the paleotemperature formula (equation 1). It shows that the current climate is the result of a long decline that started at the end of the climate optimum of the early Eocene (52 to 50 Ma ago). This decline is characterized by an increase in $\delta^{18}O$ over time that reflects the drop in ocean temperatures at higher latitudes (where deep waters are formed) in a world without major glaciers, followed by the growth of ice caps. The $\delta^{18}O$ of benthic foraminifera therefore dropped from an average of ~ 0.2 ‰ during the climate optimum of the early Eocene, to an average of ~ 4 ‰ at the end of the Quaternary.

This slow climate decline is generally attributed to two main factors: a gradual reduction in atmospheric CO_2 concentration, and the growing thermal isolation of the Antarctic continent due to the widening of the ocean passages that surround it.

Relatively abrupt incidents (that is, events happening over a much shorter time scale than the general trend), of large amplitude, are superimposed onto this slow drift, indicating that other climate drivers such as thresholds or rapid feedbacks are also involved. The first of these changes occurred at the very end of the Paleogene, at the boundary of the Eocene/Oligocene, about 33.5 Ma ago. It resulted in a rapid increase in benthic foraminiferal $\delta^{18}O$ from +1.6 to +2.8 ‰ over only 100 to 200 ka (Fig. 21.2). This change in $\delta^{18}O$ is attributed to the development of the Antarctic ice cap. The northward drift of the Australian continent allowed the opening of the Strait of Tasmania and the establishment of the Antarctic

Circumpolar Current (Zachos *et al.*, 2001). The isolation of this large land mass resulted in a drop in temperatures and the establishment of a permanent ice cap on East Antarctica, with an ice volume that may have reached about 50% of its current size. After a period of ten million years when the climate changed little, two warming phases, one at the end of the Oligocene and the other during the Middle Miocene, caused a significant reduction of the Antarctic ice sheet. The increase in temperature and the decrease in ice volume were reflected in a 1.2‰ decrease in the benthic $\delta^{18}O$ signal. The causes of these climatic changes are not clear yet.

The final phase of the climatic decline leading to the major glaciations of the Quaternary began from the Middle Miocene, between 14.2 and 12.2 Ma, and was marked by an increase in benthic foraminiferal $\delta^{18}O$ of 1.0‰ over two million years. Paleotemperature reconstructions based on Mg/Ca ratios in benthic foraminifera suggest that deep water temperature varied little, and that the growth of the Antarctic ice cap was the main contributor to the benthic $\delta^{18}O$ change (around ~0.8‰). If these estimates were correct, the ice cap located on the eastern part of Antarctica would have reached 85% of its current volume. As for the West Antarctic ice cap, it seems to have only developed from 6 Ma on, as evidenced by the first coarse sediment deposits in the Weddell Sea, coming from melting icebergs emitted at the edge of this cap. These sediments transported by drifting ice result from land erosion caused by the friction of glaciers, and are often referred to by their acronym IRD (*ice rafted debris*).

Although the development of a permanent ice cap on Antarctica started early, during the early Neogene, the development of perennial continental ice caps in the high latitudes of the northern hemisphere did not occur until the end of the Neogene. The first deposits of IRD in the Norwegian Sea, proof of the early development of an ice cap (although perhaps not a permanent one) on Greenland are not observed before 5.5 Ma (Jansen and Sjoholm, 1991). The rapid increase in $\delta^{18}O$ from ~3.2 Ma onwards may be interpreted as the beginning of permanent glaciation in high latitudes of the northern hemisphere. This glaciation intensified rapidly around 2.1 - 2.6 Ma, as evidenced by the massive IRD deposits in the Norwegian Sea.

Many studies have focused on the hypothesis of the ‘closure of the Panama isthmus’ as a potential trigger for the development of northern hemisphere ice sheets. The mechanism would involve warm intertropical waters no longer being able to cross from the Atlantic to the Pacific. They would therefore deviate into the North Atlantic, increasing oceanic evaporation in this basin and thus snow accumulation in the high latitudes. However, recent studies suggest that the closure of the Panama isthmus could have occurred during the Miocene, well before the intensification of glaciations (Montes *et al.*, 2015). The recent work of Rohling *et al.*, (2014) also observes a large temporal offset during the onset of the Plio-Pleistocene ice ages, between a marked cooling step at 2.73 My ago and the first major glaciation starting 2.15 My ago. Other theories indicate that a decrease in atmospheric CO_2 may have been responsible for a cooling, an increase of deep water formation in the North Atlantic and a change of circulation that together induced the start of the glaciations.

21.5.2 The 'Middle Pleistocene Transition' and the establishment of 100-ka cycles

The trend towards the climatic decline (seen as an increase in benthic $\delta^{18}O$) discussed in Section 21.5.1 continued over the last two million years, as is shown in detail in Figure 21.2. Superimposed on this trend are quasi-periodic oscillations. They reflect the alternating glacial periods - corresponding to a cooling of deep waters and an increase in ice volume at high latitudes - and interglacial periods, with warming and relative melting of the ice caps. It should be emphasized here that the use of the terms 'interglacial' and 'glacial' does not imply a *total* melting of ice sheets. During interglacial periods, ice sheets do not disappear, even if they are greatly reduced in the northern hemisphere. For example, during the LGM, the ice sheets in the northern hemisphere covered a large portion of North America and Europe. During the Holocene, the interglacial period we currently live in, these caps were largely diminished; the meltwater derived from them has caused sea level to rise by 120 meters since the LGM. However, an ice cap of 2.8 million km^3 continues to exist on Greenland that would cause a further sea level rise of about 7 meters, if it were to completely melt.

The amplitude of the glacial-interglacial oscillations increased sharply between 1.2 Ma and 0.6 Ma (Fig. 21.2). During this period, called 'the Middle Pleistocene Transition' (Clark *et al.,* 2006; McClymont *et al.,* 2013), a threshold response to longer-term atmospheric CO_2 decline has been proposed (Raymo *et al.,* 1997). However, recent atmospheric partial pressure CO_2 reconstructions have failed to show this long-term decrease during the Pleistocene (Hönisch *et al.,* 2009). The gradual increase in glacial-interglacial amplitude is mainly due to increasingly high values of $\delta^{18}O$ during glacial periods. The few available reconstructions of deep-water temperature during this period indicate near-freezing temperatures at every glacial maximum instead of a gradual cooling (Elderfield *et al.,* 2012), which suggests that an increase in Antarctic ice volume would be responsible for the rapid and steep increase in seawater $\delta^{18}O$ at 0.9 Ma.

This change in amplitude of glacial-interglacial oscillations is accompanied by a disruption in the frequency content of the global $\delta^{18}O$ signal. While benthic foraminifera $\delta^{18}O$ oscillations show mainly a cycle of ~41 ka over most of the Neogene and early Quaternary, the last 600,000 years are dominated by oscillations with a cyclicity of ~ 100 ka (Fig. 21.2). Some authors have agreed on the progressive nature of the 'Middle Pleistocene Transition', with the amplification of the 100 ka cycles occurring over hundreds of thousands of years. However, in some ocean regions, the records fail to demonstrate this progressive nature. This is the case, for example, in the equatorial Atlantic, where the dynamics of the thermocline, reconstructed from micropaleontological tracers, suddenly change its variability around ~930 ka. The mechanisms responsible for this transition are still unclear, although it appears that an important role can be attributed to the enormous Laurentide ice sheet, which may have favored the frequency of 100 ka through its inertia (Clark & Pollard, 1998) (see Chapter 7, Volume 2).

21.5.3 The Last Glacial Maximum (LGM)

The LGM has long been, and still remains, a major area of interest in paleoclimatology, in particular because it presents another extreme on the climate spectrum on which Earth System models can be validated (Kageyama *et al.*, 2018). Early studies defined this period as the time encompassing the last great cold maximum (as recorded by micropaleontology and pollen) as well as the maximum spread of the ice sheets (marked by the position of moraines on land masses). Radiocarbon dating has placed the maximum at around 16-20 ka ^{14}C (equivalent to 18-23 ka in calendar age). This period was the first to be the subject of a global paleoclimate study, thanks to the CLIMAP group. The isotopic maximum in $\delta^{18}O$ of planktonic and benthic foraminifera, interpreted as reflecting the cumulative effects of the cold and ice volume maxima, was used as a stratigraphic marker, and summer and winter sea surface temperatures were determined from micropaleontological transfer functions. This established the CLIMAP maps (CLIMAP 1981) (Fig. 21.3) that served as boundary conditions for the first comprehensive paleoclimate modeling experiments. The CLIMAP results have had a profound impact. For the first time, the magnitude of the temperature change between an ice age (LGM) and an interglacial period (modern times) could be quantified: the average global temperature dropped by 6 °C. However, this cooling was far from uniform: it exceeded 10 °C at high northern latitudes, while it was only a few degrees in the intertropical region. This intense cooling was associated with the development of large ice sheets over the landmasses of the northern hemisphere, which, with about 50 million cubic kilometers of ice, was the most glaciated hemisphere. In addition, analyses of Antarctic ice showed that atmospheric CO_2 concentration was about 100 ppmv below pre-industrial values (Petit *et al.*, 1999).

It quickly became necessary to expand these early studies. Continental tracers in tropical regions, such as pollen series or concentration of noble gases in aquifers (which are dependent on the temperature of the rains feeding these aquifers), indicated a cooling of 3 to 6°C during the LGM. In the nearby ocean, sea surface temperature alkenone reconstructions indicated a cooling of only about 2°C, and micropaleontological transfer functions showed little or no change. Detailed studies were therefore conducted in later decades to explain the observed differences. It appeared that many cores taken from the tropical Pacific Ocean and used for the CLIMAP reconstruction had very low sedimentation rates, so that bioturbation caused the contrasts in fauna over time to disappear. In addition, the fauna from warm waters exhibited variability that did not solely respond to temperature changes, with the result that micropaleontological transfer functions became insensitive at the temperatures above 25°C common in tropical regions. At the same time, high-resolution studies started to indicate strong climatic variability between 17 ka and 25 ka. In the North Atlantic, for example, the LGM does not correspond to the coldest conditions, which are instead associated with two periods framing the LGM: Heinrich Stadial (HS) 2 at around 24-22 ka and HS1 at around 19-17 ka.

It therefore became essential to reconsider the reconstruction of the surface ocean during the LGM. The latest and most comprehensive synthesis was carried out in the MARGO program (MARGO Project Members, 2009), which focused on the period 19-23 ka corresponding to the LGM *sensu stricto*. This period corresponds to the maximum expansion

of ice sheets, as opposed to the coldest conditions of Heinrich Stadials. The LGM MARGO reconstructions (Fig. 21.3) agree relatively well with CLIMAP, but they also revealed some important differences:

– the northern seas were ice-free during the summer;

– latitudinal and longitudinal thermal gradients were strong; the mid-latitudes of the North Atlantic Ocean experienced the strongest cooling (~ -10 °C)

– the decrease in temperature was generally larger on the eastern side than on the western side of the oceans; this was particularly marked along the African margin, especially in coastal upwelling zones of Namibia and South Africa;

– the cooling of tropical waters was close to 2°C, although some localized waters of the Pacific and Indian Oceans experienced moderated warming;

– in the Southern Ocean, a cooling of 2°C to 6°C marked a northward displacement of the polar front.

Other studies have focused on the deep ocean during the LGM. We have mentioned several of them in the description of the various methodological techniques that have been developed over the last forty years. Significant differences between the LGM and the present day include:

- the downwelling of surface waters in the North Atlantic happened in open ocean, leading to the formation of very cold deep water that found its density equilibrium at 2000 m depth;

- the very cold and dense bottom waters formed in the southern hemisphere spread throughout the deep ocean, occupying a much larger volume than today;

- the boundary between deep and bottom waters was characterized by a much stronger gradient of physical (*T*, *S*, density) and geochemical ($\delta^{18}O$, $\delta^{13}C$) properties than today;

- the ventilation and renewal rates of deep waters are still poorly constrained because of conflicting information from different tracers with a complex geochemical behavior (^{14}C, $^{231}Pa/^{230}Th$); this uncertainty is also reflected in the simulations from general circulation models of the ocean and coupled ocean-atmosphere models. Most proxies do indicate, however, lower ventilation of the deep ocean and a resulting large accumulation of carbon dioxide in the deeper waters.

21.5.4 The last deglaciation

Several decades ago, continental paleoclimatologists described the warming by steps that occurred during the last disappearance of the large northern ice caps, a period extending from 20 to 8 ka. This ‘last deglaciation’ was also identified by paleoceanographers in marine sediment cores with high sedimentation rates (Fig. 21.12). The terminology for this

succession of warming and relative cooling comes directly from the first descriptions made in the continental records based on pollen assemblages: Older Dryas, Middle Dryas, Bølling-Allerød and Younger Dryas all take their names from plant pollens (in the case of Dryas, it is associated with the reappearance of the cold flower *Dryas octopetala*), or from locations from which the samples were taken (the proglacial lake of Bølling and the city of Allerød in Denmark).

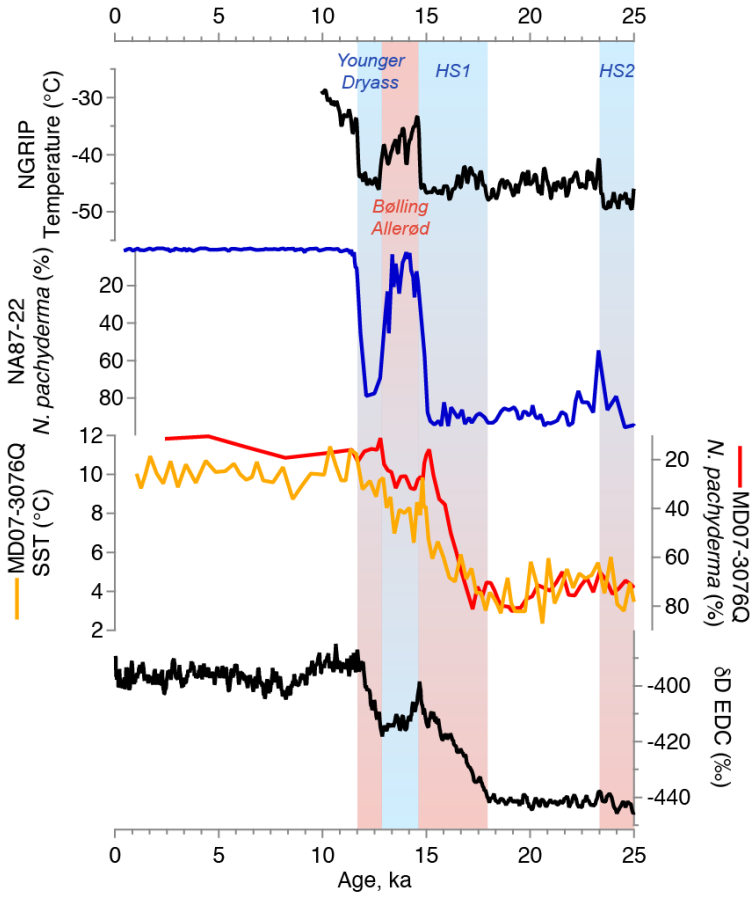

Fig. 21.12 - Records of the last deglaciation in the high latitudes of both hemispheres. (Top) Variations in $\delta^{18}O$ in the ice from the NorthGRIP site (Greenland), a proxy for the local variations in atmospheric temperature (Rasmussen *et al.*, 2014); (middle-top) Variations in the percentage of the cold species *Neogloboquadrina pachyderma* in core NA87-22 from the North Atlantic (55°30'N, 14°42'W, 2161 m deep) (Waelbroeck *et al.*, 2001; Vazquez Riveiros *et al.*, 2013); (middle-bottom) Variations in the isotopic composition of hydrogen δD of ice from Dome C (Antarctica), a proxy for local variations in atmospheric temperature (EPICA, 2004); (bottom) Variations in the percentage of the cold species *Neogloboquadrina pachyderma* and SST estimated by the Mg/Ca method in core MD07-3076Q from the Southern Ocean (44°09'S, 14°13'W, 3770 m deep) (modified from Vazquez Riveiros *et al.*, 2010).

The drivers and feedbacks that led to this specific sequence of events are still being actively studied. The start of the deglaciation is linked to the evolution of the astronomical parameters, with a strong increase in summer insolation in the northern hemisphere between 20 and 10 ka (Milankovitch's theory), and aided by pulses of increases in atmospheric CO_2 likely released from the CO_2-rich deep waters of the Southern Ocean (Marcott *et al.*, 2014).

However, the mechanisms that explain the phase differences between the two hemispheres (Figure 21.12) during the deglaciation are still unclear. A distinct warming trend appeared in Antarctica around 19 ka, while simultaneously, the northern hemisphere, after a brief warming trend, cooled and presented armadas of icebergs linked to the HS1 event (see Chapter 8, Volume 2). Following this event, around 14 ka, northern hemisphere warming was strongly amplified with a culmination during the Bølling-Allerød, while temperatures in the southern hemisphere stabilized and even dropped in Antarctica during the so-called Antarctic Cold Reversal (Figure 21.12). During this early phase of the deglaciation, the North-South antiphase is similar to what is observed during abrupt events of the last ice age, with the exception of the general deglacial warming trend. Recent studies point to CO_2 as a key mechanism of global warming during the last deglaciation. An anti-phased hemispheric temperature response to ocean circulation changes, superimposed on globally in-phase warming driven by increased CO_2 concentrations, is an explanation for much of the temperature change at the end of the most recent ice age (Barker *et al.,* 2009; Shakun *et al.,* 2012).

However, at the end of the Bølling-Allerød warm event, at about 12.5 ka, the ice caps stopped melting, the sea level stabilized and the deglaciation stopped: this was the Younger Dryas period (Figure 21.12), characterized by a return to very cold conditions for about 1.5 kyr, despite insolation reaching maximum values. This return to almost ice age conditions still raises many questions. The most commonly accepted explanation is a sudden change in the path taken by meltwater from the Laurentide ice sheet (Leydet *et al.,* 2018). Until about 12.5 ka, this huge flow of water was transported by the Mississippi River. Released into the Gulf of Mexico, the fresh water was drawn in by the circulation of the surface currents of the Atlantic (Gulf Stream followed by the North Atlantic Drift) and was very gradually diluted by the salty tropical waters without any major climate impact. During the Younger Dryas, however, the flow rate of the Mississippi River dropped considerably, which led to the hypothesis that the watershed of the meltwater plume changed and flowed instead through the St. Lawrence River to the northwest of the Atlantic Ocean. The salinity in this higher latitude area was reduced, interrupting deep water formation and thus the thermohaline circulation, and causing cooling and the growth of some glaciers. This hypothesis has been supported by simple ocean circulation models (see Chapter 5, Section 2), although marine sediment cores recovered from the likely North Atlantic zone of evacuation of meltwater have, as of yet, failed to yield traces of this event. No other satisfactory explanation has so far been proposed to explain the Younger Dryas, although the detailed study of this event could help us to better understand the interactions between ocean, ice and atmosphere under conditions of strong insolation.

21.5.5 Interglacial periods, the Holocene and the last two millennia

In order to explain the succession of glacial and interglacials periods over the last million years, Milankovitch developed the astronomical theory of paleoclimate. Since then, conceptual models have been able to describe the general trends, as well as the dominant periodicities centered around 100, 40 and 20 kyr fairly accurately (see Chapter 7, Volume 2).

Although changes in ice cap volume during glacial periods and the time constants of their response to changes in insolation are relatively well understood, the same cannot be said for the evolution of climate during interglacial periods. In particular, the mechanisms causing the differences in duration, in temperature of the atmosphere and ocean, and in ocean circulation are not well understood, even though differences in forcing are precisely calculated (Past InterGlacialS Working Group of PAGES, 2016). This lack of understanding is derived in part from the small ocean temperature differences between past interglacial periods and the present day, with temperature changes that remain close to the error of temperature reconstructions with the usual tracers (section 21.2). A further complication arises because the internal mechanisms in the climate system must be investigated through its various components (atmosphere, ocean, continent), which involves the construction of time scales common to the various archives used to reconstruct each of them, and makes the study of the interglacial periods prior to the Holocene particularly difficult.

In this section, we limit ourselves to the analysis of the last two interglacial periods: the Last Interglacial (also called the Eemian), about 125 ka ago, and the Holocene, period in which we now live. Eemian and Holocene, the terms used in this chapter, are names borrowed from palynologists to identify these two interglacial periods. A short subsection will finally be devoted to results recently obtained for the last two millennia, which has the advantage of presenting a wide range of continental and marine records that can, in some cases, be compared with recorded meteorological data.

21.5.5.1 The Last Interglacial period

Before presenting our understanding of this period of time, it is important to define what an interglacial is. It may in fact be defined in a number of ways depending on whether one considers, for example, variability in flora, ocean circulation, atmospheric temperature or ocean temperature (Past InterGlacialS Working Group of PAGES, 2016). If we take ice volume as a marker, an interglacial period *sensu stricto* is the time interval during which the ice volume is at its minimum and remains constant for several millennia.

Strictly speaking, the interglacial comparable to the period we live in, and defined by an ice volume minimum is called the Last Interglacial, and runs from about 129 to 116 ka (Govin *et al.,* 2015; Dutton *et al.,* 2015). From 115 ka, the midpoint of the transition marking the entry into MIS 5d, ice volume had already increased significantly, so much so that sea level dropped by as much as -40 m at the height of MIS 5d at about 110 ka.

During the Last Interglacial, the insolation forcing was characterized by a relatively high eccentricity, the combination of a strong inclination and a perihelion close to the summer solstice. This orbital configuration triggered an increase in summer insolation in the northern hemisphere of more than 30 W/m^2 compared to the present day. Despite these differences in forcing, the general evolution of the Last Interglacial climate is to a first degree quite similar to that of the Holocene: high temperatures at higher northern latitudes until about 123 ka (in line with higher insolation and higher elevation of the sun on the horizon), followed by a gradual cooling linked to the decline in boreal summer insolation in parallel with the

progressive growth of glacial conditions (Cortijo *et al.*, 1999). However, the Last Interglacial temperature peak was reached at about 126 ka in the North Atlantic against 129 ka in the southern high latitudes. This hemispheric asynchrony is related to the disruption of the Atlantic overturning circulation due to freshwater discharges into the North Atlantic (in response to ice sheet melting) that led to the persistence of cold conditions in the northern high latitudes and the early warming of southern high latitudes during the early phase of the Last Interglacial (Capron *et al.*, 2014; 2017).

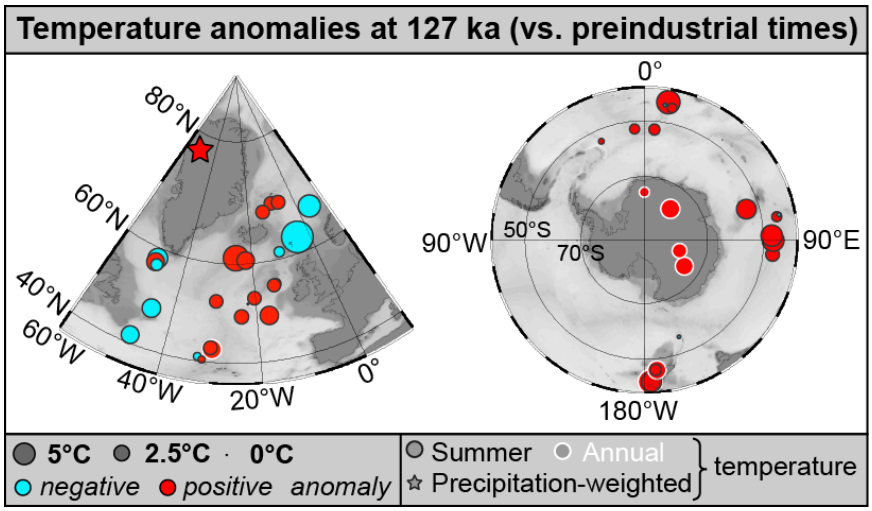

Fig. 21.13: Temperature anomalies at 127 ka compared to preindustrial times (1870-1899 CE) in the northern and southern high latitudes (modified after Capron *et al.*, 2017). Negative (positive) temperature anomalies are shown in blue (red). The bigger the dot, the stronger the temperature anomaly. Most records indicate warmer conditions at 127 ka compared to preindustrial, in response to the high boreal summer insolation. The few cold anomalies suggest remnants of freshwater discharge into the North Atlantic, Nordic Seas and Labrador Seas.

Nevertheless, despite greenhouse gas concentrations that were similar to pre-industrial times, the larger increase in summer insolation in the northern hemisphere with respect to the current situation did have an impact on the climate of the Last Interglacial optimum. Surface water temperatures were 1 to 2 °C warmer in the North Atlantic, the Nordic Seas and the Southern Ocean than during the Holocene (Capron *et al.*, 2014; 2017; Hoffman *et al.*, 2017). Such warmer high latitudes during the Last Interglacial had a double impact:

- the warming by about 0.4 °C of the temperatures of the deep Atlantic waters, which was then carried into Antarctic circumpolar deep waters (Duplessy *et al.*, 2007);

- the partial melting of Greenland and West Antarctica (Dutton *et al.*, 2015).

These two combined actions brought about a rise in sea level of 6 to 9 m (Dutton *et al.*, 2009) compared to current levels.

The Last Interglacial is a good case study to test our mechanistic understanding of the effect of warmer-than-present polar climate on sensitive components of the Earth system (e.g. ice sheets, sea level). It has recently sparked interest in the community, as shown by multiple paleo-data compilations and model-data comparison exercises (Otto-Bliesner *et al.*, 2017).

21.5.5.2 The Holocene

The Holocene period started about 10 ka ago. The last major ice sheets had not completely disappeared, but major changes had occurred since the early deglaciation, both in terms of sea level and continental and oceanic temperatures. At first look, the climate over these past 10 ka seems stable, but this apparent stability hides very pronounced regional variations in the hydrological cycle, in the circulation of surface waters (especially during the final stage of melting of the residual ice caps), and in the general circulation of the Mediterranean Sea, a basin surrounded by land and with limited connections to the open ocean and thus very strongly affected by changes in rainfall intensity over its watershed.

The Holocene is a period of major movement and development of populations. However, for the most part of this period, human activities still had a negligible impact on the global environment, so the study of climate changes over recent millennia provide a benchmark against which disturbances caused by industrial and agricultural activities can be detected. The reconstruction of Holocene climate changes is facilitated by the precise chronology offered by carbon-14 analysis.

The forcing of summer insolation at 65°N at the beginning of the Holocene reached more than 390 W/m^2 and caused a global warming that would last until about 6 ka. The temperature optimum affected the high latitudes of the North Atlantic basin, including Iceland, the Norwegian Sea and the Scandinavian coast (Koc *et al.*, 1993). In the Barents Sea, the temperature maximum was limited to the period from 7.9 to 6.9 ka due to the dissipation of the heat brought by the North Atlantic Drift by the melting of the surrounding ice. At lower latitudes, the temperature increase was accompanied by a northward shift of the Intertropical Convergence Zone (ITCZ) and a major change in monsoon dynamics, and therefore in the atmospheric water cycle. The increase in the thermal contrast between ocean and continent, for example, accentuated the African monsoon as far as the center of the continent.

The study of sediment cores from both the Mediterranean Sea and African lakes indicates the existence of major climate reorganizations. For example, before 6 ka, the Sahara was not the wide-ranging desert that it is today, but grassland dotted with lakes conducive to farming settlement. This period is called the African Humid Period (AHP). Around 6 ka, this wet period ended and conditions degraded at a rate that is still debated (Collins *et al.*, 2017; Shanahan *et al.*, 2016; Tierney *et al.*, 2015). The tropical vegetation of canopy forests along the rivers declined, and the Sahelian vegetation in turn disappeared about 2.7 ka ago to make way for the desert conditions present today. This major change could be related to the gradual decrease in insolation over the past 10 ka aided by the albedo feedback induced by the gradual disappearance of vegetation. Alternatively, a rapid termination of the AHP could have been triggered by northern-latitude cooling combined with biogeophysical feedbacks (Collins *et al.*, 2017).

During this wet period, the Mediterranean Sea received more fresh water, especially in the eastern basin (Kallel *et al.*, 1997). The sinking of well-ventilated, shallow water masses in winter became impossible in the Levantine basin, and bottom waters there became completely anoxic, leading to the disappearance of benthic fauna below 800 m depth. A layer of black

sediment rich in organic matter, called a sapropel, marks this event (Rossignol-Strick *et al.*, 1982; Rohling *et al.*, 2015). Although ventilation of the eastern waters of the Mediterranean resumed at 6 ka, the deep fauna of this basin, whose colonization rate is slow, is still very poor.

In addition to these long-term reorganizations, the Holocene also recorded an abrupt event of short duration 8.2 ka ago. Without reaching the amplitude of the rapid and sudden climate changes of the last ice age, this event still left a significant imprint on northern hemisphere temperatures. Like its glacial counterparts, the '8.2 ka event' is associated with a freshwater discharge, in this case due to the rupture of a proglacial reservoir, Lake Agassiz, formed by the retreat of the Laurentide ice sheet (Barber *et al.*, 1999; Wiersma & Renssen, 2006; Hoffman *et al.*, 2012). The sudden release of tens of thousands of km^3 of water (estimates vary from 50,000 to 120,000 km^3) over just 1 to 5 yrs had strong consequences, such as a reduction in the SST (about 1°C) and salinity of the North Atlantic, a reduction of 2 to 6°C in the atmospheric temperature above Greenland, a decrease in the temperature of air and water in the lakes of western Europe, and a decrease in the intensity of ocean circulation for a period of about 100 yrs after the freshwater discharge.

The study of the 8.2 event has shown that interglacial ocean circulation, such as the one of the early Holocene, may also be sensitive to an intense, although brief, freshwater discharge. Recent studies have pointed out that this may also have been the case during earlier interglacial periods (Galaasen *et al.*, 2014).

The climate of the last two millennia has also been the subject of much focus, since it provides a relatively long-term perspective for recent observations from the World Meteorological Organization (WMO) network (restricted to the last 150 years) and from satellites dedicated to the observation of the Earth (limited to a few decades). The reconstructions of air temperature in the northern hemisphere, used as projections for the whole planet, have primarily been based on continental data (Mann *et al.*, 1998). Reconstructing and understanding changes in the ocean over the last two millennia is particularly difficult, since oceanographic observations are only available for the last century at most, and for paleoceanographers this period is recorded in the uppermost portion of the sediment which is often poorly consolidated or lost.

Recently, much effort has been put on the gathering of the best time-series of the last two millennia as part of the Past Global Changes (PAGES) 2k network (PAGES 2k Consortium, 2017). Continental-scale temperature reconstructions provide evidence of twentieth century warming over all reconstructed regions except Antarctica (Ahmed *et al.*, 2013). A global SST compilation shows a 1800-year long cooling of the surface ocean over the pre-industrial past 2000 years (fig. 21.14), and that the cooling from 801 to 1800 CE was likely caused by volcanic eruptions (McGregor *et al.*, 2015). A more recent synthesis of paleoclimate records since 1500 CE has identified that sustained industrial-era warming of the tropical oceans first developed during the mid-nineteenth century and was nearly synchronous with Northern Hemisphere continental warming (Abram *et al.*, 2016).

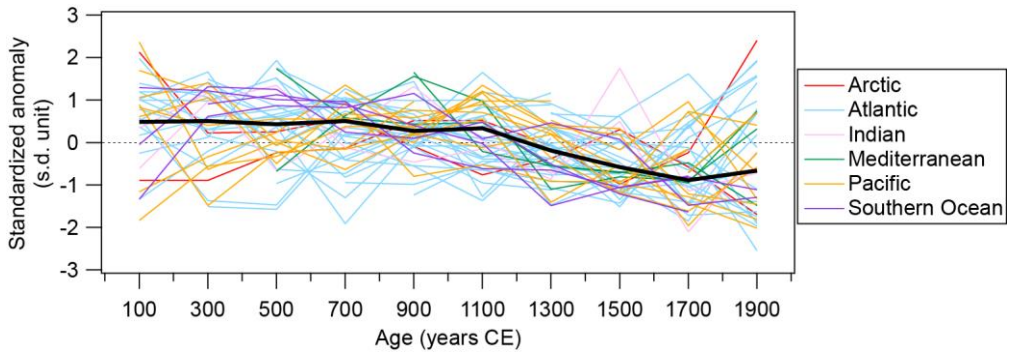

Fig. 21.14: Standardized SST anomalies over the last 2000 years (modified after McGregor *et al.*, 2015). Thin colored lines represent individual SST reconstructions from different ocean basins, which have been averaged into 200-year long bins (e.g. 1-200 CE). The thick black line is the area-weighted median SST value.

If we look at the deep ocean, the relative strength of the meridional overturning circulation has also been recently assessed for the last 1.6 ka (Thornalley *et al.*, 2018). The authors suggest that, while it was relatively stable between 400 to 1850 CE, it has declined in strength by ~15% at the beginning of the industrial era. In addition, the comparison of SST patterns in the North Atlantic with model simulations points to an additional weakening over the last 150 yrs (Caesar *et al.*, 2018).

Compilation studies like the ones presented above highlight the need for paleoclimate reconstructions, which can be compared to instrumental records that at present are too short to comprehensively assess anthropogenic climate change.

References

Abram, N.J., McGregor, H.V., Tierney, J.E., Evans, M.N., McKay, N.P., Kaufman, D.S., the Pages 2k Consortium, 2016. Early onset of industrial-era warming across the oceans and continents. Nature 536, 411, doi: 10.1038/nature19082.

Adkins, J. F., McIntyre, K. and Schrag, D. P. (2002). The Salinity, Temperature and $\delta^{18}O$ of the Glacial Deep Ocean, Science, 298, pp. 1769- 1773.

Anand, P., Elderfield, H., & Conte, M. H. (2003). Calibration of Mg/Ca thermometry in planktonic foraminifera from a sediment trap time series. Paleoceanography, 18(2).

Barker, S., Diz, P., Vautravers, M. J., Pike, J., Knorr, G., Hall, I. R., & Broecker, W. S. (2009). Interhemispheric Atlantic seesaw response during the last deglaciation. Nature, 457(7233), 1097.

Barber, D.C., Dyke, A., Hillaire-Marcel, C., Jennings, A.E., Andrews, J.T., Kerwin, M.W., Bilodeau, G., McNeely, R., Southon, J., Morehead, M.D., Gagnon, J.M., 1999. Forcing of the cold event of 8,200 years ago by catastrophic drainage of Laurentide lakes. Nature 400, 344, doi: 10.1038/22504.

Bemis, B.E., Spero, H.J., Bijma, J., Lea, D.W., 1998. Reevaluation of the oxygen isotopic composition of planktonic foraminifera: Experimental results and revised paleotemperature equations. Paleoceanography 13, 150-160.

Bintanja, R., R. S. van de Wal, and J. Oerlemans (2005), Modelled atmospheric temperatures and global sea levels over the past million years, Nature, 437, 125–128.

Böhm, E., Lippold, J., Gutjahr, M., Frank, M., Blaser, P., Antz, B., Fohlmeister, J., Frank, N., Andersen, M.B., Deininger, M., 2015. Strong and deep Atlantic meridional overturning circulation during the last glacial cycle. Nature 517, 73-76.

Caley, T., & Roche, D. M. (2015). Modeling water isotopologues during the last glacial: Implications for quantitative paleosalinity reconstruction. Paleoceanography and Paleoclimatology, 30(6), 739-750.

Capron, E., Govin, A., Stone, E.J., Masson-Delmotte, V., Mulitza, S., Otto-Bliesner, B., Rasmussen, T.L., Sime, L.C., Waelbroeck, C., Wolff, E.W., 2014. Temporal and spatial structure of multi-millennial temperature changes at high latitudes during the Last Interglacial. Quaternary Science Reviews 103, 116-133.

Capron, E., Govin, A., Feng, R., Otto-Bliesner, B., Wolff, E.W., 2017. Critical evaluation of climate syntheses to benchmark CMIP6/PMIP4 127 ka Last Interglacial simulations in the high latitude regions. Quaternary Science Reviews 168, 137-150.

Carroll, J., E. T. Brown, and W. S. Moore (1993), The role of the Ganges-Brahmaputra mixing zone in supplying barium and ^{226}Ra to the Bay of Bengal, Geochim. Cosmochim. Acta, 57, 2981–2990.

Caesar, L., S. Rahmstorf, A. Robinson, G. Feulner & V. Saba (2018) Observed fingerprint of a weakening Atlantic Ocean overturning circulation. Nature, 556, 191-198.

Chivall, D., D. M'Boule, D. Sinke-Schoen, J. S. Sinninghe Damsté, S. Schouten, and M. T. van der Meer (2014), The effects of growth phase and salinity on the hydrogen isotopic composition of alkenones produced by coastal haptophyte algae, Geochimica et Cosmochimica Acta, 140, 381–390.

Clark, P. U., & Pollard, D. (1998). Origin of the middle Pleistocene transition by ice sheet erosion of regolith. Paleoceanography and Paleoclimatology, 13(1), 1-9.

Clark, P.U., Archer, D., Pollard, D., Blum, J.D., Rial, J.A., Brovkin, V., Mix, A.C., Pisias, N.G., Roy, M., 2006. The middle Pleistocene transition: characteristics, mechanisms, and implications for long-term changes in atmospheric pCO_2. Quaternary Science Reviews 25, 3150-3184.

CLIMAP (1981) 'Seasonal Reconstructions of the Earth's Surface at the Last Glacial Maximum', Geol. Soc. Am. Map and Chart Ser., MC-36.

Collins, J.A., Prange, M., Caley, T., Gimeno, L., Beckmann, B., Mulitza, S., Skonieczny,

C., Roche, D.M., Schefuß, E., 2017. Rapid termination of the African Humid Period triggered by northern high-latitude cooling. Nature Communications 8, 1372.

Conte, M. H., Sicre, M. A., Rühlemann, C., Weber, J. C., Schulte, S., Schulz-Bull, D., & Blanz, T. (2006). Global temperature calibration of the alkenone unsaturation index (UK′ 37) in surface waters and comparison with surface sediments. Geochemistry, Geophysics, Geosystems, 7(2).

Corrège, T. (2006). Sea surface temperature and salinity reconstruction from coral geochemical tracers. Palaeogeography, Palaeoclimatology, Palaeoecology, 232(2-4), 408-428.

Cortijo, E., Lehman, S., Keigwin, L., Chapman, M., Paillard, D., Labeyrie, L., 1999. Changes in meridional temperature and salinity gradients in the North Atlantic Ocean (30-72°N) during the last interglacial period. Paleoceanography 14, 23-33, doi: 10.1029/1998PA900004.

Craig, H., and L. I. Gordon (1965), Deuterium and oxygen-18 variations in the ocean and marine atmosphere, in Stable Isotopes in Oceanographic Studies and Paleotemperatures, edited by E. Tongiorgi, pp. 9–130, Lab. Geol. Nucl., Pisa, Italy.

DeSève, A. M. (1999), Transfer function between surface sediment diatom assemblages and sea-surface temperature and salinity of the Labrador Sea, Mar. Micropaleontol., 36, 249–267.

De Vernal, A., *et al.*, (2001), Dinoflagellate cyst assemblages as tracers of sea-surface conditions in the Northern Atlantic, Arctic and sub-Arctic seas: The new n=677 data base and its application for quantitative paleoceanographic reconstruction, J. Quat. Sci., 16, 681–698.

Duplessy, J. C., N. J. Shackleton, R. K. Matthews, W. L. Prell, W. F. Ruddiman, M. Caralp, and C. H. Hendy (1984), ^{13}C record of benthic foraminifera in the Last Interglacial Ocean: implications for the carbon cycle and the global deep water circulation, Quaternary Research, 21, 225-243.

Duplessy, J. C., L. Labeyrie, A. Juillet-Leclerc, F. Maitre, J. Duprat, and M. Sarnthein (1991), Surface salinity reconstruction of the North Atlantic Ocean during the last glacial maximum, Oceanol. Acta, 14, 311–324.

Duplessy, J. C., Roche, D. M. and Kageyama,M. (2007) The Deep Ocean during the Last Interglacial Period, Science, 316, pp. 89-91.

Dutton, A., Bard, E., Antonioli, F., Esat, T.M., Lambeck, K., McCulloch, M.T., 2009. Phasing and amplitude of sea-level and climate change during the penultimate interglacial. Nature Geoscience 2, 355-359.

Dutton, A., Carlson, A.E., Long, A.J., Milne, G.A., Clark, P.U., DeConto, R., Horton, B.P., Rahmstorf, S., Raymo, M.E., 2015. Sea-level rise due to polar ice-sheet mass loss

during past warm periods. Science 349, doi: 10.1126/science.aaa4019.

Eiler, J.M., Bergquist, B., Bourg, I., Cartigny, P., Farquhar, J., Gagnon, A., Guo, W., Halevy, I., Hofmann, A., Larson, T.E., Levin, N., Schauble, E.A., Stolper, D., 2014. Frontiers of stable isotope geoscience. Chemical Geology 372, 119-143, doi: 10.1016/j.chemgeo.2014.02.006.

Elderfield, H., Yu, J., Anand, P., Kiefer, T., Nyland, B., 2006. Calibrations for benthic foraminiferal Mg/Ca paleothermometry and the carbonate ion hypothesis. Earth and Planetary Science Letters 250, 633-649.

Elderfield, H. and Ganssen, G. (2000), 'Past Temperature and d18O of Surface Ocean Waters Inferred from Foraminiferal Mg/Ca Ratios', Nature, 405, pp. 442-445.

Elderfield, H., Ferretti, P., Greaves, M., Crowhurst, S., McCave, I. N., Hodell, D. A., & Piotrowski, A. M. (2012). Evolution of ocean temperature and ice volume through the mid-Pleistocene climate transition. Science, 337(6095), 704-709.

Englebrecht, A. C., and J. P. Sachs (2005), Determination of sediment provenance at drift sites using hydrogen isotopes and unsaturation ratios in alkenones, Geochim. Cosmochim. Acta, 69, 4253–4265.

EPICA (2004) Eight glacial cycles from an Antarctic ice core. Nature, 429**,** 623-628.

Epstein, S., Buchsbaum, R., Lowenstam, H., & Urey, H. C. (1951). Carbonate-water isotopic temperature scale. Geological Society of America Bulletin, 62(4), 417-426.

Epstein, S., Buchsbaum, R., Lowenstam, H. A., & Urey, H. C. (1953). Revised carbonate-water isotopic temperature scale. Geological Society of America Bulletin, 64(11), 1315-1326.

Emiliani, C. (1955). Pleistocene temperatures, Journal of Geology, 63, 538-578.

Galaasen, E. V., Ninnemann, U. S., Irvalı, N., Kleiven, H. K. F., Rosenthal, Y., Kissel, C., & Hodell, D. A. (2014). Rapid reductions in North Atlantic deep water during the peak of the last interglacial period. Science, 343(6175), 1129-1132.

Gherardi, J. M., Labeyrie, L., Nave, S., Francois, R., McManus, J. F. and Cortijo, E. (2009). Glacial-Interglacial Circulation Changes Inferred from 231Pa/230Th Sedimentary Record in the North Atlantic Region. Paleoceanography, 24, PA2204, doi:10.1029/2008PA001696.

Ghosh, P., Adkins, J., Affek, H., Balta, B., Guo, W., Schauble, E. A., Schrag, D. P. and Eiler, J. M. (2006). ^{13}C-^{18}O Bonds in Carbonate Minerals: a New Kind of Paleothermometer. Geochimica et Cosmochimica Acta, 70, pp. 1 439-1 456.

Gottschalk, J., Vázquez Riveiros, N., Waelbroeck, C., Skinner, L.C., Michel, E., Duplessy, J.C., Hodell, D.A., 2016. Carbon isotope offsets between benthic foraminifer species of the genus *Cibicides* (*Cibicidoides*) in the glacial sub-Antarctic Atlantic.

Paleoceanography 31, 1-20.

Govin, A., Capron, E., Tzedakis, P.C., Verheyden, S., Ghaleb, B., Hillaire-Marcel, C., St-Onge, G., Stoner, J.S., Bassinot, F., Bazin, L., Blunier, T., Combourieu-Nebout, N., El Ouahabi, A., Genty, D., Gersonde, R., Jimenez-Amat, P., Landais, A., Martrat, B., Masson-Delmotte, V., Parrenin, F., Seidenkrantz, M.S., Veres, D., Waelbroeck, C., Zahn, R., 2015. Sequence of events from the onset to the demise of the Last Interglacial: Evaluating strengths and limitations of chronologies used in climatic archives. Quaternary Science Reviews 129, 1-36, doi: 10.1016/j.quascirev.2015.09.018.

Gray, W.R., Weldeab, S., Lea, D.W., Rosenthal, Y., Gruber, N., Donner, B., Fischer, G., 2018. The effects of temperature, salinity, and the carbonate system on Mg/Ca in *Globigerinoides ruber* (white): A global sediment trap calibration. Earth and Planetary Science Letters 482, 607-620, doi: 10.1016/j.epsl.2017.11.026.

Guihou, A., Pichat, S., Nave, S., Govin, A., Labeyrie, L., Michel, E. and Waelbroeck, C. (2010) Late Slowdown of the Atlantic Meridional Overturning Circulation during the Last Glacial Inception: New Constraint From Sedimentary (231Pa/230Th), Earth and Planetary Science letters, 289, pp. 520-529.

Guihou, A., Pichat, S., Govin, A., Nave, S., Michel, E., Duplessy, J.-C., Telouk, P., Labeyrie, L., 2011. Enhanced Atlantic Meridional Overturning Circulation supports the Last Glacial Inception. Quaternary Science Reviews 30, 1576-1582, doi: 10.1016/j.quascirev.2011.03.017.

Ho, S. L., & Laepple, T. (2016). Flat meridional temperature gradient in the early Eocene in the subsurface rather than surface ocean. Nature Geoscience, 9(8), 606.

Hoffman, J. S., Carlson, A. E., Winsor, K., Klinkhammer, G. P., LeGrande, A. N., Andrews, J. T., & Strasser, J. C. (2012). Linking the 8.2 ka event and its freshwater forcing in the Labrador Sea. Geophysical Research Letters, 39(18).

Hoffman, J. S., Clark, P. U., Parnell, A. C., & He, F. (2017). Regional and global sea-surface temperatures during the last interglaciation. Science, 355(6322), 276-279.

Hönisch, B., Hemming, N.G., Archer, D., Siddall, M., McManus, J.F., 2009. Atmospheric carbon dioxide concentration across the Mid-Pleistocene transition. Science 324, 1551-1556.

Hönisch, B., Allen, K.A., Russell, A.D., Eggins, S.M., Bijma, J., Spero, H.J., Lea, D.W., Yu, J., 2011. Planktic foraminifers as recorders of seawater Ba/Ca. Marine Micropaleontology 79, 52-57, doi: 10.1016/j.marmicro.2011.01.003.

Hönisch, B., Allen, K.A., Lea, D.W., Spero, H.J., Eggins, S.M., Arbuszewski, J., deMenocal, P., Rosenthal, Y., Russell, A.D., Elderfield, H., 2013. The influence of salinity on Mg/Ca in planktic foraminifers – Evidence from cultures, core-top sediments and complementary δ18O. Geochimica et Cosmochimica Acta 121, 196-213, doi:

10.1016/j.gca.2013.07.028.

Imbrie, J. et Kipp, N. G. (1971), A New Micropaleontological Method for Quantitative Paleoclimatology: Application to a late Pleistocene Caribbean Core, in Turekian, K. K. (Ed.), The late Cenozoic glacial ages, Yale University Press, pp. 71-181.

Jansen, E. et Sjoholm, J. (1991), Reconstruction of Glaciation over the 6 Myr from Ice-Borne Deposits in the Norwegian Sea, Nature, 349, 600-603.

Kageyama, M., Braconnot, P., Harrison, S.P., Haywood, A.M., Jungclaus, J.H., Otto-Bliesner, B.L., Peterschmitt, J.Y., Abe-Ouchi, A., Albani, S., Bartlein, P.J., Brierley, C., Crucifix, M., Dolan, A., Fernandez-Donado, L., Fischer, H., Hopcroft, P.O., Ivanovic, R.F., Lambert, F., Lunt, D.J., Mahowald, N.M., Peltier, W.R., Phipps, S.J., Roche, D.M., Schmidt, G.A., Tarasov, L., Valdes, P.J., Zhang, Q., Zhou, T., 2018. The PMIP4 contribution to CMIP6 – Part 1: Overview and over-arching analysis plan. Geosci. Model Dev. 11, 1033-1057, doi: 10.5194/gmd-11-1033-2018.

Kallel, N., Labeyrie, L. D., Juillet-Leclerc, A. et Duplessy, J. C. (1988) A Deep Hydrological Front Between Intermediate and Deep-Water Masses in the Glacial Indian Ocean, Nature, 333, pp. 651-655.

Kallel, N., Paterne, M., Duplessy, J. C., Vergnaud-Grazzini, C., Pujol, C., Labeyrie, L., Arnold, M., Fontugne, M. et Pierre, C. (1997) Enhanced Rainfall in the Mediterranean Region During the Last Sapropel Event, Oceanologica Acta, 20, pp. 697-712.

Keigwin, L. D., & Swift, S. A. (2017). Carbon isotope evidence for a northern source of deep water in the glacial western North Atlantic. Proceedings of the National Academy of Sciences, 114(11), 2831-2835.

Kele, S., Breitenbach, S.F.M., Capezzuoli, E., Meckler, A.N., Ziegler, M., Millan, I.M., Kluge, T., Deák, J., Hanselmann, K., John, C.M., Yan, H., Liu, Z., Bernasconi, S.M., 2015. Temperature dependence of oxygen- and clumped isotope fractionation in carbonates: A study of travertines and tufas in the 6–95°C temperature range. Geochimica et Cosmochimica Acta 168, 172-192, doi: 10.1016/j.gca.2015.06.032.

Khider, D., Huerta, G., Jackson, C., Stott, L.D., Emile-Geay, J., 2015. A Bayesian, multivariate calibration for *Globigerinoides ruber* Mg/Ca. Geochemistry, Geophysics, Geosystems 16, 2916-2932, doi: 10.1002/2015GC005844.

Kim, J.-H., van der Meer, J., Schouten, S., Helmke, P., Willmott, V., Sangiorgi, F., Koç, N., Hopmans, E.C., Damsté, J.S.S., 2010. New indices and calibrations derived from the distribution of crenarchaeal isoprenoid tetraether lipids: Implications for past sea surface temperature reconstructions. Geochimica et Cosmochimica Acta 74, 4639-4654, doi: 10.1016/j.gca.2010.05.027.

Koç, N., Jansen, E. et Haflidason, H. (1993). Paleoceanographic Reconstructions of Surface Ocean Conditions in the Greenland, Iceland and Norwegian Seas through the Last 14 Ka

Based on Diatoms, Quaternary Science Reviews, 12, pp. 115-140.

Labeyrie, L. D., Duplessy, J. C. et Blanc, P. L. (1987). Variations in Mode of Formation and Temperature of Oceanic Deep Waters over the Past 125 000 Years, Nature, 327, pp.

Labeyrie, L., Duplessy, J. C., Duprat, J., Juillet-Leclerc, A., Moyes, J., Michel, E., Kallel, N., and Shackleton, N. J. (1992). Changes in Vertical Structure of the North Atlantic Ocean between Glacial and Modern Times, Quaternary Science Reviews, 11, pp. 401-413.

Lea, D. W., Mashiotta, T. A., & Spero, H. J. (1999). Controls on magnesium and strontium uptake in planktonic foraminifera determined by live culturing. Geochimica et Cosmochimica Acta, 63(16), 2369-2379.

Leduc, G., J. P. Sachs, O. E. Kawka, and R. R. Schneider (2013), Holocene changes in eastern equatorial Atlantic salinity as estimated by water isotopologues, Earth Planet. Sci. Lett., 362, 151–162.

LeGrande, A. N., & Schmidt, G. A. (2006). Global gridded data set of the oxygen isotopic composition in seawater. Geophysical research letters, 33(12).

LeGrande, A. N., and G. A. Schmidt (2011), Water isotopologues as a quantitative paleosalinity proxy, Paleoceanography, 26, PA3225, doi:10.1029/2010PA002043.

Leydet, D.J., Carlson, A.E., Teller, J.T., Breckenridge, A., J. E., Barth, A.M., Ullman, D.J., Sinclair, G., Milne, G.A., Cuzzone, J.K., Caffee, M.W., 2018. Opening of glacial Lake Agassiz's eastern outlets by the start of the Younger Dryas cold period. Geology 46, 155-158, doi: 10.1130/G39501.1.

Lisiecki, L. E. et Raymo, M. E. (2005), A Pleiocene-Pleistocene Stack of 57 Globally Distributed d18O Records, Paleoceanography, 20, doi:10.1029/2004PA001071.

Lombard, F., Labeyrie, L., Michel, E., Spero, H.J., Lea, D.W., 2009. Modelling the temperature dependent growth rates of planktic foraminifera. Marine Micropaleontology 70, 1-7.

Lynch-Stieglitz, J., Curry, W. B. et Slowey, N. (1999) 'A Geostrophic Transport Estimate for the Florida Current from the Oxygen Isotope Composition of Benthic Foraminifera', Paleoceanography, 14, pp. 360- 373.

Lynch-Stieglitz, J., Adkins, J.F., Curry, W.B., Dokken, T., Hall, I.R., Herguera, J.C., Hirschi, J.l.J.M., Ivanova, E.V., Kissel, C., Marchal, O., Marchitto, T.M., McCave, I.N., McManus, J.F., Mulitza, S., Ninnemann, U., Peeters, F., Yu, E.-F., Zahn, R., **2007**. Atlantic Meridional Overturning Circulation During the Last Glacial Maximum. Science 316, 66-69, doi: 10.1126/science.1137127.

Lynch-Stieglitz, J., Schmidt, M.W., Gene Henry, L., Curry, W.B., Skinner, L.C., Mulitza, S., Zhang, R., Chang, P., 2014. Muted change in Atlantic overturning circulation over some glacial-aged Heinrich events. Nature Geosci 7, 144-150, doi:

10.1038/ngeo2045.

Malaizé, B., and T. Caley (2009), Sea surface salinity reconstruction as seen with foraminifera shells: Methods and cases studies, Eur. Phys. J. Conf., 1, 177–188, doi:10.1140/epjconf/e2009-00919-6.

Malmgren, B. A., Kucera, M., Nyberg, J. et Waelbroeck, C. (2001), Comparison of Statistical and Artificial Neuronal Network Techniques for Estimating Past Sea Surface Temperatures from Planktonic Foraminifera Census Data, Paleoceanography, 16, pp. 520-530.

Mann, M. E., Bradley, R. S., & Hughes, M. K. (1998). Global-scale temperature patterns and climate forcing over the past six centuries. Nature, 392(6678), 779.

Marchitto, T.M., Broecker, W.S., 2006. Deep water mass geometry in the glacial Atlantic Ocean: A review of constraints from the paleonutrient proxy Cd/Ca. Geochemistry, Geophysics, Geosystems 7, Q12003.

Marchitto, T. M., W. B. Curry, J. Lynch-Stieglitz, S. P. Bryan, K. M. Cobb & D. C. Lund (2014) Improved oxygen isotope temperature calibrations for cosmopolitan benthic foraminifera. *Geochimica et Cosmochimica Acta,* 130**,** 1-11.

Marcott, S.A., Bauska, T.K., Buizert, C., Steig, E.J., Rosen, J.L., Cuffey, K.M., Fudge, T.J., Severinghaus, J.P., Ahn, J., Kalk, M.L., McConnell, J.R., Sowers, T., Taylor, K.C., White, J.W.C., Brook, E., 2014. Centennial-scale changes in the global carbon cycle during the last deglaciation. Nature 514, 616-619.

MARGO Project Members (2009) Constraints on the Magnitude and Patterns of Ocean Cooling at the Last Glacial Maximum, Nature geoscience, DOI: 10.1038/NGEO411.

Mashiotta, T. A., Lea, D. W., & Spero, H. J. (1999). Glacial–interglacial changes in Subantarctic sea surface temperature and δ18O-water using foraminiferal Mg. Earth and Planetary Science Letters, 170(4), 417-432.

Mathien-Blard, E., Bassinot, F., 2009. Salinity bias on the foraminifera Mg/Ca thermometry: Correction procedure and implications for past ocean hydrographic reconstructions. Geochem. Geophys. Geosyst. 10, Q12011, doi: 10.1029/2008gc002353.

M'boule, D., D. Chivall, D. Sinke-Schoen, J. S. Sinninghe Damsté, S. Schouten, and M. T. van der Meer (2014), Salinity dependent hydrogen isotope fractionation in alkenones produced by coastal and open ocean haptophyte algae, Geochim. Cosmochim. Acta, 130, 126–135.

McClymont, E.L., Sosdian, S.M., Rosell-Melé, A., Rosenthal, Y., 2013. Pleistocene sea-surface temperature evolution: Early cooling, delayed glacial intensification, and implications for the mid-Pleistocene climate transition. Earth-Science Reviews 123, 173-193.

McCorkle, D.C., Martin, P., Lea, D.W., Klinkhammer, G., 1995. Evidence of a dissolution effect on benthic foraminiferal shell chemistry: $\delta^{13}C$, Cd/Ca, Ba/Ca, and Sr/Ca results from the Ontong Java Plateau. Paleoceanography 10, 699-714.

McGregor, H.V., Evans, M.N., Goosse, H., Leduc, G., Martrat, B., Addison, J.A., Mortyn, P.G., Oppo, D.W., Seidenkrantz, M.-S., Sicre, M.-A., Phipps, S.J., Selvaraj, K., Thirumalai, K., Filipsson, H.L., Ersek, V., 2015. Robust global ocean cooling trend for the pre-industrial Common Era. Nature Geoscience 8, 671-677, doi: 10.1038/ngeo2510.

McManus, J.F., Francois, R., Gherardi, J.-M., Keigwin, L.D., Brown-Leger, S., 2004. Collapse and rapid resumption of Atlantic meridional circulation linked to deglacial climate changes. Nature 428, 834-837.

Mezger, E. M., Nooijer, L. J., Boer, W., Brummer, G. J. A., & Reichart, G. J. (2016). Salinity controls on Na incorporation in Red Sea planktonic foraminifera. Paleoceanography and Paleoclimatology, 31(12), 1562-1582.

Montagna, P., McCulloch, M., Douville, E., López Correa, M., Trotter, J., Rodolfo-Metalpa, R., Dissard, D., Ferrier-Pagès, C., Frank, N., Freiwald, A., Goldstein, S., Mazzoli, C., Reynaud, S., Rüggeberg, A., Russo, S., Taviani, M., 2014. Li/Mg systematics in scleractinian corals: Calibration of the thermometer. Geochimica et Cosmochimica Acta 132, 288-310, doi: 10.1016/j.gca.2014.02.005.

Montes, C., Cardona, A., Jaramillo, C., Pardo, A., Silva, J.C., Valencia, V., Ayala, C., Pérez-Angel, L.C., Rodriguez-Parra, L.A., Ramirez, V., Niño, H., 2015. Middle Miocene closure of the Central American seaway. Science 348, 226-229.

Mulitza, S., Boltovskoy, D., Donner, B., Meggers, H., Paul, A., Wefer, G., 2003. Temperature:[delta]18O relationships of planktonic foraminifera collected from surface waters. Palaeogeography, Palaeoclimatology, Palaeoecology 202, 143-152, doi: 10.1016/S0031-0182(03)00633-3.

Müller, P. J., Kirst, G., Ruhland, G., Von Storch, I., & Rosell-Melé, A. (1998). Calibration of the alkenone paleotemperature index U 37 K′ based on core-tops from the eastern South Atlantic and the global ocean (60 N-60 S). Geochimica et Cosmochimica Acta, 62(10), 1757-1772.

Otto-Bliesner, B.L., Braconnot, P., Harrison, S.P., Lunt, D.J., Abe-Ouchi, A., Albani, S., Bartlein, P.J., Capron, E., Carlson, A.E., Dutton, A., Fischer, H., Goelzer, H., Govin, A., Haywood, A., Joos, F., LeGrande, A.N., Lipscomb, W.H., Lohmann, G., Mahowald, N., Nehrbass-Ahles, C., Pausata, F.S.R., Peterschmitt, J.Y., Phipps, S.J., Renssen, H., Zhang, Q., 2017. The PMIP4 contribution to CMIP6 – Part 2: Two interglacials, scientific objective and experimental design for Holocene and Last Interglacial simulations. Geosci. Model Dev. 10, 3979-4003, doi: 10.5194/gmd-10-3979-2017.

Ostlund, H. G. (1987). GEOSECS Atlantic, Pacific, and Indiean Ocean Expeditions Vol 7.

PAGES 2k Consortium, 2013. Continental-scale temperature variability during the past two millennia. Nature Geoscience 6, 339, doi: 10.1038/ngeo1797.

PAGES 2k Consortium, 2017. A global multiproxy database for temperature reconstructions of the Common Era. Scientific Data 4, 170088, doi: 10.1038/sdata.2017.88.

Past InterGlacialS Working Group of PAGES, 2016. Interglacials of the last 800,000 years. Reviews of Geophysics 54.

Paul, H. (2002), Application of novel stable isotope methods to reconstruct paleoenvironments: Compound specific hydrogen isotopes and pore-water oxygen isotopes, PhD thesis, 149 pp., Swiss Federal Institute of Technology.

Peral, M., Daëron, M., Blamart, D., Bassinot, F., Dewilde, F., Smialkowski, N., Isguder, G., Bonnin, J., Jorissen, F., Kissel, C., Michel, E., Vázquez Riveiros, N., Waelbroeck, C., 2018. Updated calibration of the clumped isotope thermometer in planktonic and benthic foraminifera. Geochimica et Cosmochimica Acta 239, 1-16, doi: 10.1016/j.gca.2018.07.016.

Petit, J. R., J. Jouzel, D. Raynaud, N. I. Barkov, J. M. Barnola, I. Basile, M. Bender, J. Chappellaz, M. Davis, G. Delaygue, M. Delmotte, V. M. Kotlyakov, M. Legrand, V. Lipenkov, C. Lorius, L. Pépin, C. Ritz, E. Saltzman & M. Stievenard (1999) Climate and atmospheric history of the past 420,000 years from the Vostok ice core, Antarctica. Nature, 399**,** 429-436.

Prahl, F. G. et Wakeham, S. G. (1987), 'Calibration of Unsaturation Patterns in Long-Chain Ketone Compositions for Paleotemperature Assessment', Nature, 330, pp. 367-369.

Pisias, N.G., Martinson, D.G., Moore, T.C., Shackleton, N.J., Prell, W.L., Hays, J.D., Boden, G., 1984. High resolution stratigraphic correlation of benthic oxygen isotopic records spanning the last 300,000 years. Marine Geology 56, 119-136.

Railsback, L.B., Gibbard, P.L., Head, M.J., Voarintsoa, N.R.G., Toucanne, S., 2015. An optimized scheme of lettered marine isotope substages for the last 1.0 million years, and the climatostratigraphic nature of isotope stages and substages. Quaternary Science Reviews 111, 94-106.

Rasmussen, S. O., M. Bigler, S. P. Blockley, T. Blunier, S. L. Buchardt, H. B. Clausen, I. Cvijanovic, D. Dahl-Jensen, S. J. Johnsen, H. Fischer, V. Gkinis, M. Guillevic, W. Z. Hoek, J. J. Lowe, J. B. Pedro, T. Popp, I. K. Seierstad, J. P. Steffensen, A. M. Svensson, P. Vallelonga, B. M. Vinther, M. J. C. Walker, J. J. Wheatley & M. Winstrup (2014) A stratigraphic framework for abrupt climatic changes during the Last Glacial period based on three synchronized Greenland ice-core records: refining and extending the INTIMATE event stratigraphy. *Quaternary Science Reviews,* 106**,** 14-28.

Raymo, M. E., Oppo, D. W., & Curry, W. (1997). The mid-Pleistocene climate transition: A deep sea carbon isotopic perspective. Paleoceanography, 12(4), 546-559.

Rohling, E., and G. Bigg (1998), Paleosalinity and δ18O: A critical assessment, J. Geophys. Res., 103, 1307–1318, doi:10.1029/97JC01047.

Rohling, E. J. (2000), Paleosalinity: Confidence limits and future applications, Mar. Geol., 163, 1–11.

Rohling, E. J. (2007), Progress in paleosalinity: Overview and presentation of a new approach, Paleoceanography, 22, PA3215, doi:10.1029/2007PA001437.

Rohling, E.J., Foster, G.L., Grant, K., Marino, G., Roberts, A.P., Tamisiea, M.E., Williams, F., 2014. Sea-level and deep-sea-temperature variability over the past 5.3 million years. Nature 508, 477-482.

Rohling, E. J., Marino, G., & Grant, K. M. (2015). Mediterranean climate and oceanography, and the periodic development of anoxic events (sapropels). Earth-Science Reviews, 143, 62-97.

Rosell-Melé, A., & Prahl, F. G. (2013). Seasonality of UK′ 37 temperature estimates as inferred from sediment trap data. Quaternary Science Reviews, 72, 128-136.

Rosenthal, Y., Boyle, E. A., & Slowey, N. (1997). Temperature control on the incorporation of magnesium, strontium, fluorine, and cadmium into benthic foraminiferal shells from Little Bahama Bank: Prospects for thermocline paleoceanography. Geochimica et Cosmochimica Acta, 61(17), 3633-3643.

Rossignol-Strick, M., Nesteroff, W., Olive, P., & Vergnaud-Grazzini, C. (1982). After the deluge: Mediterranean stagnation and sapropel formation. Nature, 295(5845), 105.

Saenger, C., Affek, H. P., Felis, T., Thiagarajan, N., Lough, J. M., & Holcomb, M. (2012). Carbonate clumped isotope variability in shallow water corals: Temperature dependence and growth-related vital effects. Geochimica et Cosmochimica Acta, 99, 224-242.

Schmidt, G. A., G. R. Bigg, and E. J. Rohling (1999), Global Seawater Oxygen-18 Database - v1.21. [Available at http://data.giss.nasa.gov/o18data/.]

Schmidt, G. A. (1999), Error analysis of paleosalinity calculations, Paleoceanography, 14, 422–429.

Schmittner, A., H. C. Bostock, O. Cartapanis, W. B. Curry, H. L. Filipsson, E. D. Galbraith, J. Gottschalk, J. C. Herguera, B. Hoogakker, S. L. Jaccard, L. E. Lisiecki, D. C. Lund, G. Martínez-Méndez, J. Lynch-Stieglitz, A. Mackensen, E. Michel, A. C. Mix, D. W. Oppo, C. D. Peterson, J. Repschläger, E. L. Sikes, H. J. Spero and C. Waelbroeck (2017), Calibration of the carbon isotope composition (δ13C) of benthic foraminifera, Paleoceanography, 32**,** 512-530.

Schauble, E. A., Ghosh, P., & Eiler, J. M. (2006). Preferential formation of 13C–18O bonds in carbonate minerals, estimated using first-principles lattice dynamics. Geochimica et

Cosmochimica Acta, 70(10), 2510-2529.

Schouten, S., Hopmans, E. C., Schefuß, E., & Damste, J. S. S. (2002). Distributional variations in marine crenarchaeotal membrane lipids: a new tool for reconstructing ancient sea water temperatures? Earth and Planetary Science Letters, 204(1-2), 265-274.

Schouten, S., J. Ossebaar, K. Schreiber, M. V. M. Kienhuis, G. Langer, A. Benthien, and J. Bijma (2006), The effect of temperature, salinity and growth rate on the stable hydrogen isotopic composition of long chain alkenones produced by Emiliania huxleyi and Gephyrocapsa oceanica, Biogeosciences, 3, 113–119.

Schouten, S., Hopmans, E. C., & Damsté, J. S. S. (2013). The organic geochemistry of glycerol dialkyl glycerol tetraether lipids: a review. Organic geochemistry, 54, 19-61.

Schrag, D. P., Adkins, J. F., McIntyre, K., Alexander, J. L., Hodell, D. A., Charles, C. D., & McManus, J. F. (2002). The oxygen isotopic composition of seawater during the Last Glacial Maximum. Quaternary Science Reviews, 21(1-3), 331-342.

Shackleton, N. J. (1967), 'Oxygen Isotope Analysis and Pleistocene Temperature Reassessed', Nature, 2151, pp. 15-17.

Shackleton, N. J. (1974) 'Attainment of Isotopic Equilibrium between Ocean Water and Benthonic Foraminifera Genus Uvigerina: Isotopic Changes in the Ocean during the Last Glacial' dans Les méthodes quantitatives d'étude des variations du climat au cours du Pleistocène CNRS, Gif-sur-Yvette, pp. 203-209.

Shakun, J.D., Clark, P.U., He, F., Marcott, S.A., Mix, A.C., Liu, Z., Otto-Bliesner, B., Schmittner, A., Bard, E., 2012. Global warming preceded by increasing carbon dioxide concentrations during the last deglaciation. Nature 484, 49-54.

Shanahan, T.M., Hughen, K., McKay, N.P., Overpeck, J., Scholz, C.A., Gosling, W.D., Miller, C.S., Peck, J.A., King, J.W., Heil, C.W., 2016. CO_2 and fire influence tropical ecosystem stability in response to climate change. Scientific Reports 6, 29587.

Sicre, Marie Alexandrine, *et al.*, 'Mid-latitude southern Indian ocean response to northern hemisphere Heinrich events.' Earth and Planetary Science Letters 240.3-4 (2005): 724-731.

Thierstein, H. R., Geitzenauer, K. R., Molfino, B., & Shackleton, N. J. (1977). Global synchroneity of late Quaternary coccolith datum levels Validation by oxygen isotopes. Geology, 5(7), 400-404.

Thornalley, D. J. R., D. W. Oppo, P. Ortega, J. I. Robson, C. Brierley, R. Davis, I. R. Hall, P. Moffa-Sanchez, N. L. Rose, P. T. Spooner, I. Yashayaev & L. D. Keigwin (2018) Anomalously weak Labrador Sea convection and Atlantic overturning during the past 150 years. Nature, 556, 227-232.

Tierney, J. E., Ummenhofer, C. C., deMenocal, P. B., 2015. Past and future rainfall in the

Horn of Africa. Science Advances 1.

Tierney J. E., Tingley M. P., 2018. BAYSPLINE: A New Calibration for the Alkenone Paleothermometer. Paleoceanography and Paleoclimatology 33, 281-301, doi: 10.1002/2017PA003201.

Tierney, J. E., & Tingley, M. P. (2014). A Bayesian, spatially-varying calibration model for the TEX86 proxy. Geochimica et Cosmochimica Acta, 127, 83-106.

Vázquez Riveiros, N., Govin, A., Waelbroeck, C., Mackensen, A., Michel, E., Moreira, S., Bouinot, T., Caillon, N., Brandon, M., Orgun, A., 2016. Mg/Ca thermometry in planktic foraminifera: Improving paleotemperature estimations for *G. bulloides* and *N. pachyderma* left. Geochemistry, Geophysics, Geosystems 17, 1249-1264.

Vázquez Riveiros, N., Waelbroeck, C., Skinner, L.C., Duplessy, J.C., McManus, J.F., Kandiano, E.S., Bauch, H.A., 2013. The 'MIS11 paradox' and ocean circulation: Role of millennial scale events. Earth and Planetary Science Letters 371-372, 258-268.

Vázquez Riveiros, N., Waelbroeck, C., Skinner, L.C., Roche, D.M., Duplessy, J.C., Michel, E., 2010. Response of South Atlantic deep waters to deglacial warming during Terminations V and I. Earth and Planetary Science Letters 298, 323-333.

Waelbroeck, C., Labeyrie, L., Duplessy, J. C., Guiot, J., Labracherie, M., Leclaire, H. et Duprat, J. (1998). Improving Past Sea Surface Temperature Estimates Based on Planktonic Fossil Faunas. Paleoceanography, 13, pp. 272-283.

Waelbroeck, C., J. C. Duplessy, E. Michel, L. Labeyrie, D. Paillard & J. Duprat (2001) The timing of the last deglaciation in North Atlantic climate records. Nature, 412**,** 724-727.

Weijers, J. W., Schouten, S., Spaargaren, O. C., & Damsté, J. S. S. (2006). Occurrence and distribution of tetraether membrane lipids in soils: Implications for the use of the TEX86 proxy and the BIT index. Organic Geochemistry, 37(12), 1680-1693.

Weldeab, S., D. W. Lea, R. R. Schneider, and N. Andersen (2007), 155,000 years of West African monsoon and ocean thermal evolution, Science, 316, 1303–1307.

Wiersma, A. P., & Renssen, H. (2006). Model–data comparison for the 8.2 ka BP event: confirmation of a forcing mechanism by catastrophic drainage of Laurentide Lakes. Quaternary Science Reviews, 25(1-2), 63-88.

Wit, J. C., De Nooijer, L. J., Wolthers, M., & Reichart, G. J. (2013). A novel salinity proxy based on Na incorporation into foraminiferal calcite. Biogeosciences, 10(10), 6375-6387.

Wolhowe,M. D., F. G. Prahl, I. Probert, and M. Maldonado (2009), Growth phase dependent hydrogen isotopic fractionation in alkenone-producing haptophytes, Biogeosciences, 6, 1681–1694.

Yu, E.-F., Francois, R. et Bacon, M. (1996) 'Similar Rates of Modern and Last-Glacial

Ocean Thermohaline Circulation Inferred from Radiochemical Data', Nature, 379, pp. 689-694.

Zachos, J. C., Shackleton, N. J., Revenaugh, J. S., Pälike, H. et Flower, B. P. (2001), 'Climate Response to Orbital Forcing Across the Oligocene- Miocene Boundary', Science, 292, pp. 274-278.

Zachos, J.C., Dickens, G.R., Zeebe, R.E., 2008. An early Cenozoic perspective on greenhouse warming and carbon-cycle dynamics. Nature 451, 279-283, doi: 10.1038/nature06588.

Zweng, M.M., Reagan, J.R., Antonov, J.J., Locarnini, R.A., Mishonov, A.V., Boyer, T.P., Garcia, H.E., Baranova, O.K., Johnson, D.R., Seidov, D., Biddle, M.M., 2013. World Ocean Atlas 2013, Volume 2: Salinity, in: Levitus, S., Mishonov, A.V. (Eds.). NOAA Atlas NESDIS 74, p. 39.